Published in final edited form as:
Nat Med. 2017 December ; 23(12): 1424–1435. doi:10.1038/nm.4438.

Human Primary Liver Cancer -derived Organoid Cultures for disease modelling and drug screening

Laura Broutier[1], **Gianmarco Mastrogiovanni**[#1,3], **Monique M.A. Verstegen**[#2], **Hayley E. Francies**[#4], **Lena Morrill Gavarró**[3], **Charles R Bradshaw**[1], **George E Allen**[1], **Robert Arnes-Benito**[1], **Olga Sidorova**[1], **Marcia P. Gaspersz**[2], **Nikitas Georgakopoulos**[5], **Bon-Kyoung Koo**[3], **Sabine Dietmann**[3], **Susan E. Davies**[6], **Raaj K. Praseedom**[7], **Ruby Lieshout**[2], **Jan N. M. IJzermans**[2], **Stephen J Wigmore**[8], **Kourosh Saeb-Parsy**[5], **Mathew J. Garnett**[4], **Luc J.W. van der Laan**[2], and **Meritxell Huch**[1,3,9,*]

[(1)]The Wellcome Trust/CRUK Gurdon Institute, University of Cambridge, UK [(2)]Department of Surgery, Erasmus MC-University Medical Center, Rotterdam, Netherlands [(3)]Wellcome Trust - Medical Research Council Stem Cell Institute, University of Cambridge, UK [(4)]Wellcome Trust Sanger Institute, Wellcome Trust Genome Campus, Hinxton, UK [(5)]Department of Surgery, University of Cambridge and NIHR Cambridge Biomedical Research Centre, Cambridge, UK [(6)]Department of Histopathology, Cambridge University Hospitals NHS Foundation Trust, Cambridge, UK [(7)]Department of Hepato Pancreato Biliary Surgery, Cambridge University Hospitals NHS Foundation Trust, Cambridge, UK [(8)]Department of Clinical Surgery, Royal Infirmary of Edinburgh, Edinburgh, UK [(9)]Department of Physiology, Development and Neuroscience, University of Cambridge, Cambridge, UK

[#] These authors contributed equally to this work.

Abstract

Human liver cancer research currently lacks *in vitro* models that faithfully recapitulate the pathophysiology of the original tumour. We recently described a novel, near-physiological organoid culture system, where primary human healthy liver cells form long-term expanding organoids that retain liver tissue function and genetic stability. Here, we extend this culture system to the propagation of primary liver cancer (PLC) organoids from three of the most common PLC subtypes: hepatocellular carcinoma (HCC), cholangiocarcinoma (CC) and combined HCC/CC (CHC) tumours. PLC-derived organoid cultures preserve the histological architecture, gene

[*]correspondence: m.huch@gurdon.cam.ac.uk.

Author Contributions

L.B., designed and performed experiments and interpreted results. G.M., performed experiments and interpreted results. R.A-B. and O.S. performed experiments. L.M.G., C.R.B., G.E.A. and S.D. performed bioinformatic analyses. S.E.D., performed the histopathology diagnosis. M.M.A.V., M.P.G, R.L., J.N.M.I.J., S.J.W, R.K.P., N.G. and K.S.P., provided patient material and interpreted clinical data. K.S.P., performed the kidney capsule transplants. H.E.F. and M.J.G. performed the drug screening, interpreted the results and wrote this section of the manuscript. M.H. conceived and designed the project, designed and performed experiments and interpreted results. M.H. and L.B. wrote the manuscript. All authors commented on the manuscript.

Competing Financial Interests

The authors declare no competing financial interests.

Europe PMC Funders Author Manuscripts

expression and genomic landscape of the original tumour, allowing discrimination between different tumour tissues and subtypes, even after long term expansion in culture in the same medium conditions. Xenograft studies demonstrate that the tumourogenic potential, histological features and metastatic properties of PLC-derived organoids are preserved *in vivo*. PLC-derived organoids are amenable for biomarker identification and drug screening testing and lead to the identification of the ERK inhibitor SCH772984 as a potential therapeutic agent for primary liver cancer. We thus demonstrate the wide-ranging biomedical utilities of PLC-derived organoid models in furthering the understanding of liver cancer biology and in developing personalized medicine approaches for the disease.

Primary liver cancer (PLC) is the second most lethal malignancy worldwide, with incidence rates rising, mainly due to an increase in associated risk factors like diabetes or obesity1,2. The majority of all PLC are classified into either hepatocellular carcinoma (HCC) or cholangiocarcinoma (CC)3. There is also a combined hepatocellular-cholangiocarcinoma (CHC) subtype, which accounts for 0.4 to 14.2% of all PLCs4. Albeit HCC and CC are easily distinguishable by their histological appearance2,5, genetic and transcriptional landscapes6, with CHC sharing features of both7, PLC is overall a complex entity, which renders each case of the disease unique and in need of personalized treatment.

The development of effective treatments for liver cancer has been hindered by the shortage of reproducible human models to assess the efficacy of candidate therapeutic agents8. Historically, preclinical models have mainly consisted of genetically engineered mouse models or human tumour-derived cell lines propagated in either 2D-culture or as xenografts in mice8–10. While 2D-culture has allowed pioneering advances in cancer biology, it fails to recapitulate critical features of a growing tumour *in vivo*11, specially the 3D organization. In addition, CCs have proven difficult to propagate *in vitro*12,13.

Recent reports of culture systems of primary, non-transformed tissues growing as 3D structures, termed organoids, accurately recapitulate tissue architecture and function. Thus retinal, cerebral, kidney, intestinal and stomach organoids (among others)14 have already been generated from pluripotent stem cells for the study of human development and disease. In addition, organoids are promising disease models not only for understanding the biology but also for testing drug efficacy *in vitro*, before moving to animal models15. Accordingly, mouse and human cancer organoids have recently been established for colon16–19, pancreas17,20 and prostate21 tumours, but not, thus far, from liver tumours.

Based on our previous work in mouse liver and pancreas organoid cultures22–23, we recently showed that organoid cultures derived from human liver donor/healthy tissues could be expanded long-term *in vitro* while preserving most of their liver functionality and genetic stability over time24. Here, we demonstrate the proof-of-concept that liver organoid cultures also recapitulate human primary liver cancer *in vitro*. Hence, we have successfully established organoid cultures from 8 PLC patients, encompassing three of the most common subtypes of PLC3: HCC, CC and CHC. PLC-derived organoids recapitulate the histological architecture, expression profile, genomic landscape and *in vivo* tumourigenesis of the parental tumour, even after long-term expansion in culture. In addition, we demonstrate the utility of PLC-derived organoids for identifying genes with prognostic value for PLC and

potential novel therapeutic targets, thus opening up opportunities for drug testing and advances in personalized medicine approaches.

Results

Liver cancer organoids maintain the features of the parental tumour after long-term *in vitro* expansion

We have recently established culture conditions for the long-term expansion of human cells derived from liver donor/healthy tissues24,25. Here, we sought to selectively expand tumour cells from human PLC tissue by optimizing our established human liver expansion protocol. Surgically resected liver tumour tissue was obtained from untreated PLC patients who had no history of viral-meditated hepatitis. Specimens (~1cm^3 tissue) from the 3 main PLC subtypes were obtained and each individual sample was split into 4 parts that were either processed for organoid derivation, histological diagnostic, genomic or transcriptomic analyses (Fig. 1a-b). We observed that normal/healthy contaminating tissue within the samples gave rise to organoids that would quickly outcompete the tumour-derived organoids, presumably due to differences in genetic stability, as previously suggested19. Therefore, to avoid the growth of healthy contaminating organoids, we modified our derivation protocol by (i) increasing the timing of tissue digestion, which reduced the yield of healthy contaminants; (ii) changing the starting culture conditions using, in addition of the classical isolation medium24,25, a newly defined PLC-derived organoids isolation medium consisting in the classical isolation medium24,25 without R-spondin-1, Noggin and Wnt3a but supplemented with Dexamethasone and Rho-kinase inhibitor for at least 2 weeks (Fig. 1c) and (iii) closely monitoring the developing organoid structures. Particularly, for all the samples in the manuscript we cultured half of the cell suspension in classical isolation medium and the other half in our tumouroid specific isolation medium, to ensure growth of the cultures (Supplementary Fig. 1 & methods). At the first passage all cultures (healthy and tumour, irrespective of their subtype-of-origin) were transferred to our previously defined "human healthy liver-derived organoids expansion medium"24,25 and expanded and maintained in this medium.

Using this novel protocol, we successfully established human PLC-derived organoids from 8 different PLC patients, including poorly differentiated to moderate/well differentiated HCC (n=3) and CC (n=3), and combined HCC/CC (CHC; n=2) (Fig. 1, Supplementary Fig. 2a and Supplementary Table 1). We found a strong correlation between the derivation success rate (establishment) and the proliferation index of the original tumour. Thus, the efficiency of establishment of organoid cultures was 100% for those samples derived from tumours that contained > 5% proliferating cells (n=3 for HCC; n=2 for CHC and n=3 for CC), while we did not succeed in deriving organoids from very well differentiated lesions, with <5% proliferative cells in the original samples (n=8 for HCC and n=1 for CC), in agreement with the histological grading of early HCCs5 (Supplementary Fig. 2b-g and Supplementary Table 1).

PLC-derived organoids (termed "tumouroids" henceforth) from all 3 different subtypes expanded long-term (~1year) in culture, with a consistent passaging ratio of 1:3-1:4 every 7-10 days. HCC-2, though, stopped growing after ~1 month, due to fibroblasts outcompeting

the tumouroids growth, which precluded any downstream analysis. Therefore, we have performed all the downstream analysis on the remaining 7 lines and corresponding patient's tissues (HCC-1 and -3; CHC-1-2 and CC-1-3) (Fig. 1d and Supplementary Fig. 2h).

At the histological level, tumouroids presented patient-specific heterogeneous morphologies ranging from solid/compact structures (HCC and CHC) to more irregularly-shaped cyst-like structures (CC) in contrast to the ordered, homogeneous, cyst-like hollow structure of healthy liver-derived organoids (Fig. 1b and SupplementaryFig. 2a). These morphological features allowed individual samples to be distinguished from each other, both within and between subtypes, even at late passage and after having been cultured for months in the same conditions.

We then sought to determine whether the 3D-tumouroids would retain the histological features of the patient tumour tissue. Healthy liver-derived organoids form single-layered epithelial structures that transition into a pseudo-stratified epithelium upon differentiation (see ref 24 for details). In contrast, the tumouroids exhibited a very different histological and cellular architecture, which recapitulated the histological features of the patient's tissue and tumour subtype. Thus, HCC and CHC tumouroids exhibited a solid, filled 3D structure with HCCs, but not CHCs, also forming pseudoglandular rosettes, typical of HCC3,7. Similarly, CC tumouroids exhibited extensive glandular domains with carcinoma cells invading the lumen and growing in cribriform structures, as observed in the patient's tissue (Fig. 1b and Supplementary Fig. 2a).

Detailed histological and marker analysis of all the patient's tumour tissues revealed that our cultures derived from a moderate/well differentiated HCC (HCC-1; AFP+/HepPar1+), a poorly differentiated HCC (HCC-3; AFP+/HepPar1-), a classical combined (CHC-1; AFP±/HepPar1+/EpCAM+/mucin+), a combined with stem cell features (CHC-2; AFP+/HepPar1+/EpCAM+/mucin-) and poorly to moderate/well differentiated CCs (CC-1-3; HepPar1-/EpCAM+) (Fig. 2a-b, Supplementary Fig. 3a-c and Supplementary Table 1)26. Subsequent analysis of these subtype-specific markers in the tumouroids revealed that these express the diagnostic markers of their parental tissues, even after long-term expansion in culture in the same culture conditions. Thus, EpCAM, was highly expressed in all CCs (CC-1-3) and CHCs (CHC-1-2) tumouroids and corresponding patients' tissues, but absent on HCCs tumouroids and tissues (Fig. 2c and Supplementary Fig.3b). Likewise, AFP a well-established marker for HCCs and a subset of CHCs27, but not expressed in CCs3,5,28–29, was highly expressed in both HCCs and CHC-2 tumouroids, in agreement with the expression pattern of the original patient's tissue (Fig. 2c and Supplementary Table 1). Remarkably, *SALL4* described for a subset of poorly differentiated HCCs30–31 and CHCs32 was only present in HCC-3 and CHC-2, both in tumouroids and matching tissues (Supplementary Fig. 3d).

Overall, these results demonstrate that liver tumouroids both recapitulated and retained the histological characteristics and marker expression of the original tumour tissue and subtype, even after long-term expansion in culture, in the same culture conditions.

Primary Liver Cancer-derived organoid cultures recapitulate the expression profile of the corresponding tissue-of-origin and tumour subtype

The gene expression patterns of PLC subtypes (HCC, CC and CHC) have been extensively studied33–34. Therefore, to further characterize our tumouroid cultures we compared their expression profiles to the corresponding parental tissues using genome-wide transcriptomic (RNAseq) analysis. Healthy liver-derived organoid lines and corresponding tissues were used as additional controls.

Relative transcript abundance (transcripts per million, RPKM) of 15,648 gene transcripts was determined. Principal component analysis (PCA) analysis indicated that both technical and biological replicates per patient were almost identical (Supplementary Fig. 4a-b and Supplementary Dataset 1). Therefore, we present the data per patient as average of all these replicates. A first hierarchical clustering analysis comparing the gene expression profiles of our tissue samples with publically available TCGA PLC cohorts (344 HCC and 31 CC samples) confirmed that the samples used in this study are representative of the overall population of primary liver cancer (Supplementary Fig. 4c and Supplementary Dataset 1). Then, we compared the expression profiles of these parental tissues to the corresponding tumouroid lines. Gene expression correlation analysis indicated that each tumouroid line correlated to its corresponding tissue-of-origin but not with the other subtypes (Fig. 3a). Along the same line, organoids and tissue samples grouped by subtype on the PC2 component, while the PC1 component accounted for the variance between tissues and tumour-derived organoids. Classical HCC/hepatocyte markers35 such as *AFP* or *APOH* and CC/ductal markers36 such as *KRT7*, were amongst the genes that contributed the most to the variance in the PC2 component (Fig. 3b and Supplementary Dataset 1).

When evaluating specific tumoural/differentiation markers, we found that the tumouroids' expression profiles resembled the corresponding matching tissues and subtype (Supplementary Fig 4d). Notably, we found the HCC markers (*AFP* and *GPC3*) and hepatocyte markers (*ALB, TTR, APOA1, APOE*) to be highly expressed in our HCC tumouroids and matching tissue while CC/ductal markers were amongst the most downregulated. Reciprocally, CC markers such as *EPCAM*, *KRT19* or *S100A11*2,37,38–39 were highly expressed in our CC lines and tissues, while HCC markers were not expressed or strongly downregulated. The CHC lines shared the expression pattern of both, as expected (Fig. 2b-c, Fig. 3b-c, Supplementary Fig. 3b, Supplementary Fig. 4d and Supplementary Fig. 5a-b), and Supplementary Dataset 1). Remarkably, the expression pattern was also retained in a patient-specific manner even within each subtype. For instance, *MUC5B* was expressed only in CHC-1 but not in CHC-2 organoids, in agreement with the corresponding patient's tissue (Supplementary Dataset 1 and Supplementary Fig. 3c), whereas AFP was expressed in CHC-2 but not CHC-1 in concordance with the AFP values in serum of these patients at the moment of resection (compare Fig. 2c and Supplementary Table 1).

These results were confirmed by global analysis using Gene-Set-Enrichment-Analysis (GSEA) of the tumouroid lines and their corresponding parental tissues against 159 published cancer gene-sets (Fig. 3d and Supplementary Datasets 2 and 3). Thus, for both HCC lines and corresponding tissues, HCC gene-sets were the most significantly positively enriched, with HCC-1 associated to gene-sets describing HCC with hepatocyte

differentiation features while HCC-3 significantly associated with a proliferative HCC subclass and a KRT19 positive subclass gene-sets in agreement with the differentiation status of the patient's original tissue. Conversely, for all CC tumouroids and matching tissues, CC gene-sets were the most significantly positively enriched whereas HCC specific gene-sets were significantly down-regulated, as expected. Similarly, the CHC expression profiles were negatively correlated with HCC-differentiation gene-sets but positively correlated with progenitor/stem cell, proliferation and/or poor prognosis gene-sets (Fig. 3d, Supplementary Fig. 5c-d and Supplementary Dataset 2 and 3).

Subsequent analyses confirmed the RNAseq results, with HCC but not CC tumouroids exhibiting hepatocyte differentiation features (ALB and HNF4a expression, Albumin secretion, and production of bile acid in the medium (the later for HCC-1)) (Supplementary Fig. 5b, e-f). In contrast, KRT19, marker for CC, CHC tumours2,27 and a subset of HCCs26, was highly expressed in all CC (CC-1-3), in both CHC (CHC-1-2) and in HCC-3 derived tumouroids, but undetectable in HCC-1, in agreement with the histological subtype, expression pattern and gene signature of the patient's tumour tissue (Supplementary Fig. 5a-b and d). Moreover, *KRT7*, a well-established marker for CCs37, was only expressed in the CC-derived organoids and corresponding tissues (Supplementary Fig. 5f).

These results demonstrate that the PLC-derived organoid culture system faithfully recapitulates and maintains the transcriptomic alterations present in the individual patient's tumour subtype. Since the different tumour subtypes were all maintained in the same culture conditions these results suggest that their tumour signature is intrinsic to the cancer population, and is not significantly modified by the culture conditions.

Tumouroid/Organoid cultures enable the identification of potential prognostic biomarkers for primary liver cancer

We next sought to investigate if the tumouroid culture system could represent a valuable resource to identify novel genes involved in PLC and/or novel potential PLC biomarkers, a use not previously described for any patient-derived organoid system. For that, we defined a "tumouroid signature" list by comparing the similarities between the transcriptomes of all tumouroid lines to healthy liver-derived organoid lines. Notably, within the top 30 most upregulated genes we found 19 genes already reported to be markers/overexpressed in PLC, 13 of which were already associated to poor-prognosis, while the remaining 11 genes had never been associated to PLC (Fig. 3e and Supplementary Dataset 1).

We then performed an in-depth analysis of these top 30 genes by determining their expression pattern and prognostic value in cohorts of primary liver cancer patients and healthy individuals from publically available TCGA databases (for HCC: 374 HCC patients and 50 healthy individuals; for CC: 31 CC patients and 8 healthy individuals). Notably, 29 of the top 30 genes were significantly ($p \leq 0.01$) overexpressed in cancer patients *vs* healthy individuals for both cohorts. Importantly, from the 11 novel genes never associated before to liver cancer, 4 exhibited poor survival prognosis when overexpressed: *C19ORF48, UBE2S* and *DTYMK* (for HCC) and *C1QBP* (for CC). Of note, *STMN1*, previously associated to HCC but not CC40, also predicted poor survival in the CC-cohort (Fig. 3f-h and Supplementary Dataset 1). Therefore, these results demonstrate that growing primary liver

cancer as tumouroids preserves the tumour-cell features at a level that allows identifying new genes with a prognostic value and that could potentially be used as prognostic biomarkers for primary liver cancer.

Liver tumouroids retain the genetic alterations present in the original tumour tissue

PLCs typically present with a high degree of aneuploidy, several copy number changes, somatic mutations and epigenetic alterations6. All the lines that we expanded in culture (HCC, n=2; CHC, n=2; CC, n=3) exhibited multiple chromosomal aberrations consisting of both gains and/or losses of chromosome numbers (Fig. 4a-b). This was in stark contrast to healthy liver-derived organoids that stably maintained diploid chromosome numbers in culture, in agreement with our previous observations24,41. To determine whether the different tumouroid lines retain the parent tumour's mutational landscape, we performed whole exome sequencing (WES) analysis of each line expanded for short (<2 months, early passage) or extended (>4 months, late passage) periods in culture and compared the results to the corresponding parent tumour.

We generated ~19 Gb exome DNA sequence data from each sample. When comparing the global variant profile, we observed that, on average, ~92% of the variants in the patient's tissue were retained in the corresponding early tumouroid cultures (<2months), and >80% even after months of expansion (Fig. 4c). Similarly, the analysis of the proportion of exonic variations for both patient's tissue and corresponding cultures confirmed that both, single nucleotide variants (SNVs) and Indels in the original tissue, are well retained in culture. Also, the distribution of base substitutions for both tissues and tumouroids revealed an over-representation of the T>C/A>G and C>T/G>A transversion, in agreement with the mutational spectrum described for CCs and HCCs42–43 (Fig. 4d-e). Of note, we did not find significant bias between transcribed and untranscribed strands (Supplementary Fig. 6a).

Since we lacked matched germline (normal/non-tumour) mutational data, in order to select for cancer related variants we filtered for variants present in COSMIC and excluded polymorphisms by using publically available databases following the guidelines described in ref 44 (see methods). The majority of all the cancer-related somatic variants present in the patient's original tissue were retained in the corresponding tumouroid cultures (~84%). In fact, <16% (in average) were lost between tissue and early tumouroids, thus suggesting that the cultures represent the tumour genetic landscape of the original patient, with little bias of tumouroids cells harbouring specific mutations (~0.5 % in average) (Fig. 4f). The total number of deleterious mutations that could impact protein function ranges from 70 to 294, in agreement with published mutational burdens for HCC and CC tumours42,45 (Supplementary Fig. 6b, Supplementary Dataset 4).

Next-generation sequencing studies have created a detailed map of the genetic alterations present in liver cancer and its subtypes6. In agreement with this mutational spectrum, HCC-1 line and corresponding patient tissue exhibited missense mutations in *CTNNB1* (Fig. 4g and Supplementary Dataset 4), consistently with their significant enrichment in CTNNB1 mutated liver cancer gene-set found in the gene GSEA (Fig. 3d) and their elevated levels of Wnt target genes (Supplementary Dataset 1). CHC-2 line harboured a *TP53* frameshift variant (L206fs). Also, we identified an activating mutation in *KRAS* (*KRASG12D*) in CC-1

and CHC-1 tumouroid lines and matching tissues, but not in the HCC lines, in agreement with the significant enrichment in EGF activated gene-set for those lines (Supplementary Fig. 6c)46. We also found nonsense mutations and a disruptive deletion in the chromatin remodelling genes *ARID1A* (HCC-3 and CC-1) and *ARID2* (HCC-3), in agreement with previous reports where both genes are altered in all subtypes of PLC47–48 (Fig. 4g, and Supplementary Dataset 4). As expected, all lines were devoid of mutations in *MAPK1* and *MAPK3* (ERK1 and ERK2 respectively), as described for PLC45.

Therefore, these results indicate that the PLC tumouroid culture system retained the mutational landscape of the original tumour tissue and faithfully retained the tumour subtype specific mutations present in the original sample from which where derived.

Tumouroids recapitulate the histology of the parental tumour and show metastatic potential *in vivo*

To determine whether tumouroids also recapitulate the features of a human primary liver tumour *in vivo*, we transplanted CC (CC-1-3 lines) and HCC-1 long-term expanded tumouroids under the skin of immunocompromised mice. Healthy liver-derived organoids were used as controls (Fig. 5a). We found tumour outgrowths in the animals engrafted with CC-1_O (29/29), CC-2_O (8/8) and HCC-1_O (24/34), but not when injected with healthy liver-derived organoids (Healthy-1_O) (Fig. 5b and Supplementary Fig. 7a-b). The CC-derived tumours exhibited a strong stromal reaction with CC-1_O tumours forming glands with proliferative cells growing in cribriform structures (Fig. 5c Supplementary Fig. 7c, and CC-2_O exhibiting a more differentiated phenotype (Supplementary Fig. 7 d), reminiscent of the corresponding patient's tumour tissue. Similarly, HCC-1_O derived tumours grew as a solid mass with proliferative cells (Supplementary Fig. 7c) and exhibited pseudoglandular rosettes, as in the patient's tissue (Fig. 5d). Secondary tumouroids derived from these xenografted tumours exhibited similar chromosome counts and were morphologically and histologically indistinguishable from their parental line (Supplementary Fig. 7e-f). Hence, this indicated that even after long-term expansion *in vitro* and transplantation *in vivo*, expanding primary liver tumours in organoid culture, stably preserves the histological architecture of the parent tumour.

Primary liver cancer has been reported to metastasize primarily to the lung and portal lymph nodes49. To determine whether our tumouroid models would faithfully recapitulate liver cancer metastatic phenotype, we injected CC-1_O, derived from a patient with history of metastasis, into the kidney capsule of NSG mice. As expected, 100% of the injected mice developed tumours that resembled the original patient tissue (Fig. 5b and e). More importantly, in 7 out of 9 injected mice we found lung metastases, in agreement with the patient's diagnostic at the moment of resection (Supplementary Table 1), while, as expected, healthy liver-derived organoids (Healthy-1_O) did not generate any metastases (Fig. 5b and f, Supplementary Fig. 7 g-h)

Overall, these results establish that primary liver cancer-derived organoids accurately model the histological and metastatic features of their parent tumours *in vivo,* even after long-term expansion in culture.

Europe PMC Funders Author Manuscripts

Liver tumouroids allow the identification of patient-specific drug sensitivities and uncover ERK as a potential target for primary liver cancer

We performed proof-of-concept drug sensitivity testing in 6 of the PLC tumouroids lines (HCC-1; HCC-3; CHC-1,-2; CC-1,-2) to evaluate their use to identify patient-specific sensitivities and as a platform to inform drug development. As an initial prioritization step, for each tumouroid line we tested their sensitivity to 29 anti-cancer compounds, including drugs in clinical use or development. Tumouroids were treated with a dilution series of each compound for 6 days, before measuring cell viability50. Drug sensitivity was represented by the area under the dose response curve (AUC) and by the half-maximal inhibitory concentration (IC_{50}) (Fig. 6a-c and Supplementary Dataset 5). The assay was conducted with technical replicates and two biological replicates per tumouroid were independently screened. There was a positive correlation of biological AUC replicates ($R_p = 0.79$) and IC_{50} replicates ($R_p = 0.73$) across the dataset. CC-2 was insensitive to all compounds and so was excluded from further analyses.

From our initial prioritization screen, we confirmed drug sensitivity for a subset of compounds using a tumouroid formation assay, thus validating our screening method. We selected clinically relevant compounds where differential sensitivity was observed across the tumouroid panel; namely Taselisib, Gemcitabine, AZD8931, SCH772984 and Dasatanib (Fig. 6c-d). Overall, a good agreement between the screening and validation results was observed (Supplementary Fig. 8a). For instance, Taselisib resulted in a growth inhibitory effect in 5 of 6 tumouroids while Dasatinib suppressed tumouroid formation only in CC-1 cells, both results in agreement with our screening results. An exception was for CC-1 line with AZD8931, where we observed a variable sensitivity between biological replicates in the prioritization screen (Fig. 6 c-d, Supplementary Fig. 8a).

Overall, tumouroids were resistant to the majority of the compounds, with an IC_{50} greater than the maximum screening concentration, although we detected interesting sensitivity to several compounds demonstrating a correlation between some drug sensitivities and mutational profiles in the tumouroid lines. For instance, HCC-1 harbouring mutations in *CTNNB1* gene, was resistant to the porcupine inhibitor LGK974, whereas CC-1, Wnt-dependant tumour (Fig.1c), was sensitive (Fig. 6a-c). Moreover, EGFR-family inhibition with AZD8931 restricted tumouroid formation in HCC-1 cells (wild-type for *KRAS*), whereas the other lines, and notably CC-1 and CHC-1 (*KRAS* mutants) were resistant. Interestingly we also observed tumouroid sensitivity to Gemcitabine, which is used clinically for the treatment of PLC patients (Fig. 6a-c).

Of particular interest was the substantial inhibition of tumouroid formation following inhibition of ERK1/2 by SCH772984 in HCC1-3, CC-1 and CHC-1 cells (Fig. 6a-d and Supplementary Fig. 8a). SCH772984, which selectively inhibited ERK-phosphorylation in HCC-1 and CC-1 tumouroids (Supplementary Fig. 8b), was effective in lines that were insensitive to the BRAF and/or MEK inhibitors in our screen (Dabrafenib and Trametinib) (Fig. 6c). The reason for this difference is unclear, although ERK inhibitors have demonstrated activity in cells with acquired BRAF and MEK inhibitor-resistance51.

We note that clinical trials exploring the effect of specific ERK inhibitors for PLC have not been reported thus far. Hence, to further investigate the potential of ERK1/2 inhibition for PLC, we tested the efficacy of SCH772984 to inhibit tumour growth *in vivo*. For that, CC-1 and HCC-1-derived tumouroids were transplanted subcutaneously into NSG mice and, when tumours reached ~100mm3, those were injected intra-tumourally with either SCH772984 or the vehicle. Remarkably, 2-7 days after the first injection we observed a significant reduction in tumour growth, which lasted for the remainder of the experiment (Fig. 6e and Supplementary Fig. 8c). Histological analysis revealed that the tumour mass was necrotic and that the majority of the cells were apoptotic (Fig. 6f-g and Supplementary Fig. 8d). Western blot analysis confirmed that SCH772984 also *in vivo* selectively inhibited ERK-phosphorylation in CC-1 tumours (Supplementary Fig. 8e). Thus, in aggregate, our proof-of-concept study demonstrates the application of PLC tumouroids for *in vitro* and *in vivo* drug testing, and provides initial evidence that ERK inhibition could have a beneficial therapeutic effect on a subset of HCC and CC patients.

Overall, these results indicate that by faithfully retaining the histological, transcriptomic and genomic landscape of their parent tumour, tumouroid cultures facilitate the prediction of drug sensitivity/resistance in a patient-specific manner. Therefore, they provide an important new resource for liver cancer research, opening up new avenues for biomarker discovery and drug testing.

Discussion

The advent of 3D culture systems has made it possible to partially recapitulate the complexity and function of mammalian tissue *in vitro*, by forming structures that resemble an adult organ in culture and which have been termed “organoids”14. We recently have demonstrated that gastric, pancreatic and hepatic organoid cultures derived from adult tissues self-renew and differentiate *in vitro*, into the corresponding cell types of the tissue-of–origin14–15.

Here, we demonstrate the proof-of-concept that primary liver cancer (PLC) tissue grown as organoid cultures (here termed tumouroid) faithfully models the genetic complexity of human PLC *in vitro*. We successfully established cultures from tumours derived from 8 PLC patients representing the three most common subtypes of PLC3: HCC, CC and CHC. In contrast to any liver cancer cell line grown in 2D, PLC-derived organoids recapitulate the histological architecture and expression profiles of the corresponding parent tumour, even after long-term expansion in the same culture conditions for all subtypes or upon transplantation into mice. Notably, they also retain the specific differences between patients as well as between tumour subtypes. We have exploited this aspect here to demonstrate the proof-of-concept that tumour-derived organoid cultures could represent a valuable resource for biomarker discovery, especially for prognostic markers, an application not previously reported for any organoid culture system. We report *C19ORF48, UBE2S, DTYMK* (for HCC) and *C1QBP* and *STMN1* (for CC) as all novel genes associated to poor prognosis for primary liver cancer. Further studies, though, will be necessary to prove their utility as prognostic or their relevance as predictive biomarkers and/or their potential direct

involvement in the progression of the disease. These results open up novel opportunities in using tumour-derived organoids for tumour marker discovery.

A unique and important feature of the tumouroids is that they maintain the mutational landscape of the original patient's tumour, even after long-term expansion in culture. This is vastly different to existing 2D cell lines, which albeit they cover the major driver mutations observed in many cancer sub-types52, no longer present the patient-specific signature and genetic landscape of the original tumours from whence they were derived, exemplified by the frequent acquisition of mutations in *TP53* in such cell lines53. The reasons for these differences are unknown, but it is feasible to speculate that the cell-matrix interactions may play an important role. In fact, embedding primary tumoural epithelial cells within an extracellular matrix (ECM) enables the cells to interpret the environment and self-assemble into structures which acquire tissue patterning, as it occurs during development and organogenesis. Also, the cell-matrix interactions established in 3D could prevent anoikis-apoptosis due to detachment from the matrix54- of those tumoural cells that have not acquired yet all the mutations to survive in a ECM-free milieu, thus facilitating the maintenance of heterogeneous, non-selected populations within the culture. In that line, our results indicate that if selection of specific tumoural cells exist in the cultures, this might have a minor effect at the population level, as we found that tumouroids harbour >92% of the SNVs present in the original tissue.

The reproduction of parent tumour genetic aberrations in a culture setting makes tumouroid lines a potentially valuable resource in screening drug sensitivity/resistance, identifying novel players in primary liver cancer, or even novel therapeutics as part of a personalized medicine approach. Our results validate such an approach by (1) demonstrating a correlation between some drug sensitivities and the mutational profile in the tumouroid lines and (2) the *de novo* identification of the ERK inhibitor SCH772984 as a potential novel therapeutic agent for PLC. Future studies aiming at validating the efficacy of ERK inhibition in a bigger collection of tumouroid lines will be required, though, to confirm its therapeutic value for liver cancer.

The lack of immune system and stromal components, though, represents a limitation of the culture system, especially when aiming at studying tumour cell-stroma/immune interactions. In that regard, patient derived xenografts (PDXs) have proven useful models for human cancer, including liver cancer13,55, as they also retain tumour histopathology, including tumour-infiltrating lymphocytes and the stromal component, and global gene expression and methylation profiles of the patient's malignant epithelial cells56. However, PDXs suffer from a low engraftment rate, especially CCs (5.8% engraftment efficiency as reported by Cavalloni et al.,13), have a long engraftment period (often several months), are expensive and time-consuming, and are not tractable for large-scale drug sensitivity testing56. Therefore, we believe that the PLC-derived organoid cultures we present here are complementary and alternative models to liver cancer PDXs. Furthermore, they are suitable for large-scale drug testing, and in a timescale that makes it potentially compatible with personalized medicine approaches.

In conclusion, the PLC-derived organoids that we present here fulfil all the criteria of a reliable *in vitro* cancer model, recapitulating all the features of three of the most common subtypes of liver tumours, from histological architecture to genetic and transcriptomic traits, and are amenable as a platform for drug screening. With a short timescale from establishment to drug testing, this novel *in vitro* primary liver cancer system thus makes hitherto inaccessible possibilities for predicting patient-specific drug responses and creating personalized/*à la carte* therapies into a reality.

Online Methods

General experimental approaches

No samples, mice or data points were excluded from the reported analyses. Detailed information on experimental design and reagents is available through the accompanying Life Sciences Reporting Summary and Supplementary Dataset 6. Raw data used to generate figures are provided in Datasets 1-6 and Source data files 1 and 2.

Human specimens

Liver tumour specimen (~1-4 cm3) were obtained from resection performed at Erasmus Medical Center Rotterdam (MEC-2013-143), Cambridge University Hospitals NHS Trust (REC: 15/LO/0753 - Approval by NRES Committee London – Westminster) and The Royal Infirmary Hospital Edinburgh (REC: 15/ES/0097) on patients who had no history of viral-meditated hepatitis (excluded under Institutional safety guidelines). Handling and processing of samples was performed according to HTA guidelines. Healthy liver resections (~1cm3) were obtained during liver transplantation performed at the Erasmus Medical Center, Rotterdam MEC-2014-060 and at the Cambridge University Hospitals NHS Trust REC: 15/EE/0152. The Cambridge samples were provided by the Cambridge Biorepository for Translational Medicine (CBTM). All patients provided informed consent. Samples were procured and the study was conducted under Institutional Review Board approval prior to tissue acquisition. Samples were confirmed to be tumour or normal based on histopathological assessment. The diagnosis of each case was confirmed on routine hematoxylin and eosin-stained slides by an independent histopathologist. For each tumour specimen, samples were split into 4 parts and processed for histology, RNA and DNA isolation, or dissociated and processed for organoid culture.

Isolation and Culture of human liver healthy and tumoural organoids

Healthy liver-derived organoids were isolated and cultured using our previously described method24,25 while tumour-derived organoids (tumouroids) were isolated by adapting this method as follows. Briefly, ¼ of the patient-derived or healthy donor specimen (~0.25 to 1cm3) was minced and incubated at 37°C with the digestion solution. Incubation was performed for 30min-1h for healthy donor tissue (as described in ref 24) while for patient-derived tissue digestion was left for 2-5 hours to overnight (O/N) according to the degree of liver fibrosis, which was evaluated in a patient-specific basis by visual inspection under a stereomicroscope as well as according to the resistance of the tissue to be minced. For patient-derived tissue, after 2-5h digestion, the digestion preparation was visually inspected and either digestion was stopped or, if a significant part of the original tissue was still under-

digested (>50% of starting material, depending on the fibrotic status of the tissue), the preparation was left o/n at 37°C in the digestion solution, in order to get a good yield of tumoural cells. This increase in the digestion times compared to healthy tissue (>2h-o/n) facilitated reducing the number of viable healthy contaminating duct cells. In all cases, the digestion was stopped once no pieces of tissue were left, and the suspension was then filtered through a 100μm nylon cell strainer and spun 5 min at 300-400G. The pellet was washed in cold Advanced DMEM/F12 (GIBCO) then mixed with BME (Basement Membrane Extract, Type 2, Pathclear). 2.000-5.000 cells were seeded per well in a 24-multi-well plate. After BME had solidified, half of the wells obtained for each sample were cultured in the classical human liver organoid isolation medium (Advanced DMEM/F12 supplemented with 1% Penicillin/Streptomycin, 1% Glutamax, 10 mM HEPES, 1:50 B27 supplement (without Vitamin A), 1:100 N2 supplement, 1.25mM n-Acetyl-L-cysteine, 10% (vol/vol) Rspo-1 conditioned medium, 30% (vol/vol) Wnt3a conditioned medium, 10mM nicotinamide, 10nM recombinant human [Leu15]-Gastrin I, 50ng/ml recombinant human EGF, 100ng/ml recombinant human FGF10, 25ng/ml recombinant human HGF, 10μM Forskolin, 5μM A8301, 25ng/ml Noggin and 10μM Y27632 as described in ref 24). The other half were cultured in a tumouroid specific isolation medium (classical human liver organoid isolation medium without Noggin, Rspo-1 and Wnt3a conditioned media but supplemented with 3nM Dexamethasone (Sigma Aldrich). Thus, the tumoroid isolation medium contained: Advanced DMEM/F12 supplemented with 1% Penicillin/Streptomycin, 1% Glutamax, 10 mM HEPES, 1:50 B27 supplement (without Vitamin A), 1:100 N2 supplement, 1.25mM n-Acetyl-L-cysteine, 10mM nicotinamide, 10nM recombinant human [Leu15]-Gastrin I, 50ng/ml recombinant human EGF, 100ng/ml recombinant human FGF10, 25ng/ml recombinant human HGF, 10μM Forskolin, 5μM A8301, 10μM Y27632 and 3nM Dexamethasone). It is important to always culture half of the sample in classical isolation medium and half in our tumouroid specific isolation medium, to ensure growth of the cultures. For instance, CC-1 patient material only grew in classical isolation medium because it requires Rspo-1 to grow. For this line, though, we enriched for the tumouroids by hand-picking out contaminating healthy organoids (as described in Supplementary Fig. 1).

After isolation medium was changed twice a week. For healthy-donor derived organoids, isolation medium was changed to “human healthy liver-derived organoids expansion medium” after 1-week in culture (see composition below). For tumouroids, isolation medium (classical or tumouroid specific) was maintained until the first split. For tumouroid culture establishment, after 2-3 weeks in culture (depending on the sample) the growing structures were visually inspected and, if required, contaminating healthy organoids were hand-picked to prevent these from outgrowing the tumouroid structures. Upon attainment of dense culture (healthy liver-derived organoids (1-2 weeks after isolation) and tumour-derived organoids (2-3 weeks after isolation) were passaged by mechanical dissociation into small fragments via trituration with a glass Pasteur pipet, and transferred to fresh matrix in the previously defined “human healthy liver-derived organoids expansion medium”24,25 : Advanced DMEM/F12 supplemented with 1% Penicillin/Streptomycin, 1% Glutamax, 10 mM HEPES, 1:50 B27 supplement (without Vitamin A), 1:100 N2 supplement, 1.25mM n-Acetyl-L-cysteine, 10% (vol/vol) Rspo-1 conditioned medium, 10mM nicotinamide, 10nM recombinant human [Leu15]-Gastrin I, 50ng/ml recombinant human EGF, 100ng/ml

recombinant human FGF10, 25ng/ml recombinant human HGF, 10μM Forskolin and 5μM A83-01)24. Expansion medium was changed twice a week and cultures were split upon attainment of dense culture.

All cultures were tested every month for mycoplasma using the 'PCR Mycoplasma Test kit I/C' kit from Promega in accordance with the manufacturer's instructions.

To prepare frozen stocks, organoid cultures were dissociated and mixed with recovery cell culture freezing medium (GIBCO) and frozen following standard procedures. When required, the cultures were thawed using standard thawing procedures and cultured as described above. For the 3-4 days (organoids) or first 2 weeks (tumouroids) after thawing, the culture medium was supplemented with Y-27632 (10μM). Organoid pictures were taken with either a Leica M80 stereoscope and Leica MC170 HD camera or with an inverted microscope Leica DMIL and Leica DFC 450C camera.

Histology and staining

Tissues and organoids were fixed for 24 or 0.5 hours respectively, in 10% neutral buffered formalin (Sigma), at room temperature, and then embedded in paraffin as follows: briefly, tissues were processed through a graded ethanol series followed by xylene, and then embedded in paraffin, cut at 5μm and stained (H&E and immunohistological staining). For immunofluorescence experiments fixed organoids were rehydrated with PBS following formalin fixation. For immunohistological staining, paraffin slides were deparaffinised and subjected to antigen retrieval using citrate sodium solution pH=6. To reduce background nonspecific staining, and permeabilise the sample, slides were incubated with a 3% BSA, 0.5% Triton in TBS solution for 1 hour. Primary antibodies (listed in the Supplementary Dataset 6) were then applied at appropriate dilutions for overnight at 4°C (see Supplementary Dataset 6 for details). Endogenous peroxidase activity was blocked for 15 min in a 3% hydrogen peroxide/methanol buffer. Detection of bound antibody was accomplished with the BrightVision Ultimate kit (Immunologic). Briefly, slides were washed in TBS and incubated with a secondary antibody-HRP conjugate for 1 hour at room temperature and finally developed with 3,3′-diaminobenzidine (DAB) for 5 min, counterstained with haematoxylin, and mounted with DPX (Sigma). Slides were also stained in the absence of primary antibodies to evaluate nonspecific secondary antibody reactions. For TUNEL assay, Click-iT Plus TUNEL kit (Molecular Probes, Life technologies) was used in accordance with the manufacturer's instructions. Pictures were taken with a Leica microscope DM 4000 microscope and DFC 450 camera (Leica). For whole mount immunofluorescence staining, organoids were processed as described in 23,24 25. Briefly, organoids were incubated over 2 to 3 nights at 4°C, washed in PBS, and revealed by incubation with a secondary antibody conjugated to a fluorophore. Nuclei were stained with Hoechst33342 (Molecular Probes, Life technologies). Confocal images were captured on a Leica SP5 inverted confocal microscope (Leica).

Ki67 index

Each tumour slide stained for Ki67 was manually scanned with a microscope at ×10 objective, and the area of greatest Ki67 positivity (hot spot) was selected for photographing.

At least 1000 total tumoural cells were counted on a total of 2 independently stained slides per patient. Pictures were taken with a Leica microscope DM 4000 microscope and DFC 450 camera (Leica) and Ki67-negative and -positive were then counted using ImageJ “cell counter” plugin. Light brown or pale staining nuclei were ignored during counting.

Karyotyping

Karyotyping was performed as previously described 24. Briefly, cultures were incubated with 0.1ug/ml Karyomax Colcemid (Gibco). After 24 hours, organoids were harvested and dissociated using TrypLE (Gibco). Cells were incubated with KCL 0.0075M hypotonic solution for 10 min, fixed in methanol:acetic acid (3:1) and dropped on a microscope slide for visualization. Nuclei were mounted and stained using Vectashield with DAPI (Vector Labs). A minimum of 15 metaphases per sample were counted.

Sequencing and analysis

For both RNA-Sequencing (RNASeq) and Whole-Exome Sequencing (WES), low quality reads were filtered (<Q20) followed by trimming of low quality bases from the ends of the reads (<Q20). Adaptors were also removed using cutadapt.

RNA-Sequencing—RNA was isolated from organoids using RNeasy mini kit (Qiagen) following manufacturer's instructions. RNA libraries were prepared for sequencing using the Smartseq2 method. RNA sequencing was performed using Illumina HiSeq sequencer (50bp single-end reads and 10-20 million reads were generated for each sample). Reads were aligned with Tophat (v2.1.0)57 to the GRCh38.82 genome, using the corresponding gtf file for exon positions. Counts were generated using featureCounts (v1.5.0-p1)58. Only protein-coding genes, lincRNAs, processed transcripts and misc RNA were kept for further study. Normalised counts were created using DESeq259 and RPKMs using edgeR's function [edgeR]. The technical and biological replicates (different passages) were merged. Healthy growing in expansion and differentiation medium and corresponding tissues were used as additional controls.

To assess concordance of tissues with organoids genes were filtered and the Pearson’s correlation coefficient was calculated pairwise between tissues and organoids. The correlation matrix was then z-scored. The principal components for several subgroups of the samples were calculated from the normalised DESeq counts, and the first two (PC1, PC2) were plotted. We then analysed the top 100 genes with highest loadings across PC2, which separated the samples by subtype. Functional analysis was split across the three subtypes, and genes were excluded in each unless healthy or tumour samples had RPKM values greater than 1. To generate a statistic for tumoural tissue samples, the log2 fold change (FC) of each tumoural tissue was divided by the mean of the healthy tissues. To generate a statistic for HCC tumouroid samples, two log2 fold changes (FC) were calculated: the first was HCC organoid divided by the mean of healthy liver-derived organoid and the second was HCC tissue divided by the mean of the healthy tissues. Then the mean or minimum was then taken of these two ratios, whichever had a lower absolute value. The same statistic was generated for CHC and CC tumouroids using the mean healthy tissue instead of healthy liver-derived organoid as a baseline for the first fold change. These statistics were then used

for pre-ranked gene set enrichment analysis using GSEA software (http://www.broadinstitute.org/gsea/)60. 159 gene sets were used for running the GSEA. These gene sets were obtained after curation of the publically available C2 MSigDB collection for "LIV", "HEPT" and "STEM" key words and completed by available liver cancer gene set described in literature (see Supplementary Dataset 2 and 3) in order to select a relevant list of gene sets associated with liver cancer and stemness. 1,000 permutations were used to calculate p-value. A tumouroid signature was identified by finding genes with the highest FC when dividing the minimum expression value, in RPKMs, over all tumouroid samples by the mean of the expression of healthy liver-derived organoids in differentiation medium. Several aspects of the genes defining the tumouroids' signatures were annotated: the description of their corresponding proteins was downloaded from Uniprot61, and their relevance to disease by retrieving the Disease Ontology terms (using the R package dnet v1.0.1062).

WES—DNA from tumour tissue and matched tumouroid lines was extracted using DNeasy Blood & Tissue Kit (Qiagen) according to manufacturers' protocol. Point mutations and short indels were called in a procedure composed of several steps as follows: **(i)** Reads were aligned to the UCSC hg38 genome using Bowtie2 (v2.2.6)63 and the output was preprocessed for variant calling by marking duplicates with Picard (v1.113) (http://broadinstitute.github.io/picard/) followed by Indel realignment with the GATK toolkit (v3.7)64. SNPs and Indels were called with Varscan (v.2.3)65. **(ii)** We identified and selected the variants with the following parameters: base quality ≥15 (Phred score), read depth ≥15 and annotated by SNPEff66 as not "intergenic". **(iii)** We removed variants on alternate haplotypes. **(iv)** Analysis was then split between patients. For each, there were 3 samples, the tissue and the corresponding tumouroids expanded for <2months (early) or >4months (late). If a variant was called in the 'early' sample, a variant was added in the tissue if its pileup showed evidence of the same variant at that position. Moreover if a variant was called in the 'late' sample, a variant was added in the tissue and early sample if their pileup both showed evidence of the same variant at that position. Fig. 4c-e and Supplementary Fig. 5a are based on this final list of variants. To assess concordance, overlaps of variants found in tissue and early and late tumouroids were calculated within and between cancer types using GATK (v3.7). The mutation spectrum was examined in each sample in both non-transcribed and transcribed strands and then summarized by representing the average proportion across all samples. A cancer-related set of variants was defined by adding the following filtering steps: **(v)** To filter out polymorphisms and non-damaging variants we exclude variants which had reads supporting variations ≥2 in our sequenced healthy samples (Healthy-1_Tissue and _Organoid; Healthy-2_Organoid) and / or were included in dbSNP (common _ no _ known _ medical _ impact _ 20170801.vcf)67 and / or with a frequency >0.01 in ExAC database68. To select for cancer related variants we then **(vi)** filter for the variants present in COSMIC (v76)69, and **(vii)** synonymous and intronic variants were filtered out. The variant positions with their associated effects were annotated with SnpEff66. Resultant variants were used for the Fig. 4f. **(viii)** Finally, we selected the mutations that were highly predicted to impair the function of the corresponding encoded proteins by filtering for coding mutations and using SIFT70) to predict the deleterious (SIFT score <0.05) impact of missense and structural variants. A summary of the concordant (tissue/early/late) coding variants obtained per

patient is provided in Supplementary Dataset 4 and this final list of variants was used for Supplementary Fig. 6b and Fig. 5g.

Accession Numbers

All RNA-seq and WES data are available at Gene Expression Omnibus (GEO) under accession number GSE84073.

https://www.ncbi.nlm.nih.gov/geo/query/acc.cgi?acc=GSE84073

The Cancer Genome Atlas (TCGA) analyses

We used public available data generated by the TCGA Research Network: http://cancergenome.nih.gov/ to perform hierachical clustering and survival outcome analyses. FPKMs were downloaded from the Genomic Data Commons Data Portal (GDC), using GDC's API, for the projects TCGA-LIHC (374 tumoral samples (ICD-O-3 number=C22.0) and 50 normal control samples) and TCGA-CHOL (31 tumoral samples (ICD-O-3 number=C22.1) and 8 normal control samples).

For the hierarchical clustering our sequencing data was processed according to the GDC mRNA quantification analysis pipeline to obtain FPKM values comparable with the ones from the TCGA-cohorts. The hierarchical clustering used the Euclidean distances between samples based on the top 500 expressed genes and was performed using hclust in R and plotted using the dendextend R package71. Healthy, not annotated for the stage of the disease and recurrent disease samples were excluded from the analysis.

For the survival analysis we examined the expression of the top 30 genes of the tumouroid signature, in both TCGA-LIHC and TCGA-CHOL cohorts. From the FPKM values of tumoral and control samples we generated base R boxplots (R's default boxplot code) and assess the significance between both group by unpaired two-tailed t-test. Survival plots were created using the R package TCGAbiolinks (v2.2.10)72 and by splitting, per gene, the tumour samples into high- and low-expression groups. The median of all samples was used as the threshold and significance for differences between the two groups was assessed by log-rank test.

Quantitative RT-PCR

Total RNA was extracted from organoid cultures or freshly isolated tissues using RNeasy mini kit (Qiagen) in accordance with the manufacturer's instructions. cDNA was synthesized using 0.5μg of total RNA and a M-MLV Reverse Transcriptase kit (Promega). cDNA was amplified with iTaq™ Universal SYBR Green Supermix (BioRad) and using gene-specific primers described in Supplementary Dataset 6). All targets were amplified (40 cycles) on a CFX96 Touch Real-Time PCR Detection System (Biorad). Data were analyzed using BioRad CFX manager. Expression levels were normalized to the expression of the housekeeping gene HPRT.

Europe PMC Funders Author Manuscripts

Functional *in vitro* studies

Functional studies were performed in collected supernatant or in whole organoids. To assess albumin production, culture medium was collected 1 week after the last medium change and albumin levels were assessed using an Albumin ELISA kit (Assay Pro) according to manufacturer's instructions. Values were corrected for time and cell number. Concentration of total bile acid was established using a Total Bile Assay kit (Cell Biolabs, inc.) according to manufacturer's instructions on supernatant obtained after sonication of whole organoids in PBS.

Organoid formation Assay

To assess the organoid formation efficiency in classical *vs* tumouroid isolation medium, pictures of all full drops of BME obtained per patient were photographed using a Leica M80 stereoscope 2-3 weeks after isolation (depending on the sample) and all viable tumouroid structures were counted.

For the drug sensitivity assays, organoids were dissociated into 2-5 cell clumps by enzymatic dissociation with TrypLE (Life Technologies). Then, cell viability assays were conducted by plating 500 clumps per well of a 48-well cell culture plate in 250µl of expansion medium supplemented with 0.5 µM Gemcitabine (Actavis), or 5 µM of AZD8931 (Selleckchem), or 10µM of SCH772984 (Selleckchem) or 2µM Dasatinib (Selleckchem) or 10µM of Taselisib (Selleckchem) or 3µM of IWP2 (Sigma Aldrich) or 1µM of Gefitinib (Selleckchem) or vehicle (DMSO) control. All conditions were supplemented with Rho kinase inhibitor Y-27632 (Sigma-Aldrich). The concentration selected for each compound was based on the cell viability data from our laboratory, the results from the screening or the literature. Medium was changed 3 times a week for 3 weeks. Viable cells were assessed by their ability to generate organoid *de novo*. Representative pictures of the viability result were taken 2-3 weeks after starting the treatment. All cell viability experiments were conducted in triplicate in at least two independent experiments (biological replicates = different passages).

Drug screening

Organoid viability assays were conducted as previously described19,50. Briefly, 8µl of ~7mg/ml BME-2 was dispensed in to 384-well microplates and allowed to polymerize. Organoids were mechanically dissociated by pipetting before being resuspended in 2% matrigel/growth media (15.000-20.000 organoids/ml) and dispensed into 384-well plates. The following day a concentration dilution series of each compound was dispensed using liquid handling robotics and cell viability assayed using CellTiter-Glo® (Promega) following 6 days of drug incubation. An experimental concentration range was calculated for each compound using a 7-point half-log dilution series of the highest maximal concentration. The maximal concentration of each compound can be found in Supplementary Dataset 5. Screens were performed in technical (same screening run) and biological duplicates (different passage), and all screening plates were subjected to stringent quality control measures and a Z-factor score comparing negative and positive control wells was calculated. Dose–response curves were fitted to the luminescent signal intensities utilizing a method previously described73. Variation in replicates was greater than similar screens performed in colorectal tumouroids and was likely due to the large size of HCC tumouroids leading to uneven

distribution in screening wells19,50. Compound and screening concentrations are provided in Supplementary Dataset 5. The range of concentrations selected for each compound was based on *in vitro* data of concentrations inhibiting relevant target activity and cell viability based on data from our laboratory or literature.

Mouse xenograft studies

All mouse experiments have been regulated under the Animals (Scientific Procedures) Act 1986 Amendment Regulations 2012 following ethical review by the University of Cambridge Animal Welfare and Ethical Review Body (AWERB) and have been performed in accordance to the Home Office license awarded to M.H. For subcutaneous grafts, 1 million cells suspensions were prepared in PBS-0.1%BSA (CC and healthy liver-derived organoid lines) or in Advanced DMEM/F12 (GIBCO) 1% glycosil (ESI-BIO) further supplemented with 50 ng/ml each of HGF and VEGF (HCC and healthy liver-derived organoid lines) and were injected into both flanks of male NSG-NOD scid gamma mice (Charles River). Visible tumours developed in approximately 2–4 weeks (CC organoid lines) and 4-6 months (HCC-1 organoid line). Mice were culled when the tumour reached limit end-point (size or ulceration). For kidney capsule graft, cell line suspensions were prepared in Advanced DMEM/F12 (GIBCO) with BME2 (7mg/ml) and 500.000 cells were implanted under the renal capsule of NSG mice. These mice were then culled at different time point (0.5, 1, 2 and 3 month) and kidney and lung tissues were harvested to assess the growth and the metastatic potential of the grafted cells.

To assess the efficiency of the ERK inhibitor SCH772984 *in vivo* mice with established subcutaneous tumours were randomized to drug treatment by splitting size-matched tumours in two groups (SCH772984/vehicle). Treatments (SCH772984 at 2 mg/kg, or an equal volume of vehicle (25%DMSO-30%PEG300 in DD water) were administered by intratumoural injection twice daily for 15 (CC-1 tumouroid line) or 20 (HCC-1 tumouroid line) days. Tumour sizes were measured 3 times a week after the first week of treatment using a caliper and volumes were calculated by applying the formula $v = 0.5 \times L \times w \times h$, where v is volume, L is length, w is width and h is height. Investigators performing tumour measurements were blinded to treatment groups. Histological analyses of the tumours from both CC-1 and HCC-1 lines were performed at 24 and 25 days after treatment initiation respectively.

Western blot assay

Cell lysate for Western blotting were prepared from **(i)** ice-cold PBS washed tumouroids (to remove the basement matrix) grown for 24 hours in expansion medium supplemented with 10μM of SCH772984 (Selleckchem), or 5 μM of AZD8931 (Selleckchem) or equal volume of vehicle (DMSO) and from **(ii)** CC-1 xenografted tumours, 6 hours after intratumoural injection of 2mg/kg of SCH772984 (Selleckchem) or equal volume of vehicle. Lysates were made in ice-cold buffer consisting of 50mM Tris-HCl (pH 7.4), 150mM NaCl, 2mM EDTA, 50mM NaF, 1% triton, 1% NP-40. 0.1% SDS, 0.5% Na-deoxycholate, supplemented with 1mM sodium orthovanadate and protease inhibitor cocktail (Roche) (15min on ice for the cells and 30min on ice for the tissues). Protein lysates were cleared by microcentrifugation at 10.000 rpm for 10 min at 4°C and the supernatants aliquoted and stored at −20°C.

Equivalent amounts of protein from each sample were separated on 10% SDS-PAGE gels and then transferred by electroblotting onto nitrocellulose membranes. Membranes were then blocked in in PBS-0.1% Tween-5% BSA and immunoblotted with the following antibodies overnight at 4°C: ERK (1/2000), P-ERK (1/3000) (Cell signalling). After washing 3 times in PBS-0.1% Tween, the membranes were incubated for 1h at room temperature with anti-rabbit horseradish peroxidase (HRP)-conjugated secondary antibodies (1:10.000; abcam). Antibody-protein complexes were visualised using ECL Prime Western Blotting Detection Reagent (GE Healthcare).

Statistical Analyses

All summary data are presented as mean ± SD or representative images of at least 2 independent experiments. All statistical analyses were performed in R and GraphPad Prism software (GraphPad 7.0). Sample size (n) values used for statistical analyses are provided in the relevant figures and supplementary figures. Individual data point are graphed or can be found in Source data files. Tests for differences between two groups were performed using Mann-Whitney's two-tailed test, Student's two-tailed unpaired t-test or log-rank test as specified in the figure legends. When using t-test we assumed normality and equal distribution of variance between the different groups. No data points were excluded from the statistical analyses. Significance was set at FDR ≤0.25 (for GSEA) and p-value ≤0.05 (for all other experiments).

Supplementary Material

Refer to Web version on PubMed Central for supplementary material.

Acknowledgements

M.H. is a Wellcome Trust Sir Henry Dale Fellow and is jointly funded by the Wellcome Trust and the Royal Society (104151/Z/14/Z). L.B. is supported by an EMBO Postdoctoral fellowship (EMBO ALTF 794-2014) and Marie-Curie Postdoctoral fellowship (Grant 656193_H2020-MSCA-IF-2014). G.M. was supported by a Marie Curie Initial Training Network (Marie Curie ITN WntsApp 608180) and a H2020 LSMF4LIFE grant (ECH2020-668350). This work was funded by an NC3Rs International prize, a Beit Prize, a Cambridge Cancer Center-pump priming award (CRUK-RG83267) and, partially, by a NC3Rs project grant (NC/R001162/1), all of them awarded to M.H. Work at the L.J.W.v.d.L lab was funded by the research program InnoSysTox, [project number 114027003], by the Netherlands Organisation for Health Research and Development (ZonMw) and part of the research program financed by the Dutch Digestive Foundation [MLDS-Diagnostics project number D16-26]. Work in the MJG lab is funded by the Wellcome Trust (102696), Stand Up To Cancer (SU2C-AACRDT1213), and Cancer Research UK (C44943/A22536).

We thank Dr Clare Pacini for help with the clustering analysis of the HCC and CC TCGA-cohorts and the samples used in this study. We also thank Ms Cora Olpe and Mr Nicholas Hircq for help in the early phases of the project, Dr Chris Hindley for editorial assistance, The Gurdon Institute facilities for help with imaging and animal care, Dr. Sylviane Moss, Dr Maike Paramor and Dr Joaquin Martinez for assistance with sequencing analysis and Dr Asif Jah (Cambridge University Hospitals NHS Trust) and Dr Jeroen de Jonge (Erasmus Rotterdam Center) for facilitating recruitment of patients. Finally, M.H. would like to thank Prof Brigid Hogan (Chapel Hill) and Prof Magdalena Zernicka-Goetz (University of Cambridge) for helpful discussions and critical comments.

References

1. Bosch FX, Ribes J, Díaz M, Cléries R. Primary liver cancer: Worldwide incidence and trends. Gastroenterology. 2004; 127:S5–S16. [PubMed: 15508102]
2. Bridgewater J. Guidelines for the diagnosis and management of intrahepatic cholangiocarcinoma. Journal of Hepatology. 2014; 60:1268–1289. [PubMed: 24681130]

3. Hirohashi, S., et al. Tumours of the Liver and Intrahepatic Bile Ducts. World Health Organization Classification of Tumours. Stanley, R.Hamilton, MD.Lauri, A., Aaltonen, MD., PhD, editors. IARCPress; 69372 Lyon France: 2000.
4. Lee SD, et al. Clinicopathological features and prognosis of combined hepatocellular carcinoma and cholangiocarcinoma after surgery. Hepatobiliary Pancreat Dis Int. 2014; 13:594–601. [PubMed: 25475861]
5. International Consensus Group for Hepatocellular, N. Pathologic diagnosis of early hepatocellular carcinoma: A report of the international consensus group for hepatocellular neoplasia. Hepatology. 2009; 49:658–664. [PubMed: 19177576]
6. Marquardt JU, Andersen JB. Liver cancer oncogenomics: opportunities and dilemmas for clinical applications. Hepatic oncology. 2015; 2:79–93. [PubMed: 26257864]
7. Wang A-Q, et al. Combined hepatocellular cholangiocarcinoma: Controversies to be addressed. World Journal of Gastroenterology. 2016; 22:4459–4465. [PubMed: 27182157]
8. Sharma SV, Haber DA, Settleman J. Cell line-based platforms to evaluate the therapeutic efficacy of candidate anticancer agents. Nat Rev Cancer. 2010; 10:241–253. [PubMed: 20300105]
9. De Minicis S, et al. Liver carcinogenesis: Rodent models of hepatocarcinoma and cholangiocarcinoma. Digestive and Liver Disease. 2013; 45:450–459. [PubMed: 23177172]
10. Oikawa T, et al. Model of fibrolamellar hepatocellular carcinomas reveals striking enrichment in cancer stem cells. Nature Communications. 2015; 6:8070.
11. Shamir ER, Ewald AJ. Three-dimensional organotypic culture: experimental models of mammalian biology and disease. Nature reviews Molecular cell biology. 2014; 15:647–664. [PubMed: 25237826]
12. Ku JL, et al. Establishment and characterisation of six human biliary tract cancer cell lines. British Journal of Cancer. 2002; 87:187–193. [PubMed: 12107841]
13. Cavalloni G, et al. Establishment and characterization of a human intrahepatic cholangiocarcinoma cell line derived from an Italian patient. Tumour Biology. 2016; 37:4041–4052. [PubMed: 26486326]
14. Huch M, Koo B-K. Modeling mouse and human development using organoid cultures. Development. 2015; 142:3113–3125. [PubMed: 26395140]
15. Hindley CJ, Cordero-Espinoza L, Huch M. Organoids from adult liver and pancreas: Stem cell biology and biomedical utility. Developmental Biology.
16. Crespo M, et al. Colonic organoids derived from human induced pluripotent stem cells for modeling colorectal cancer and drug testing. Nat Med. 2017; 23:878–884. [PubMed: 28628110]
17. Li X, et al. Oncogenic transformation of diverse gastrointestinal tissues in primary organoid culture. Nature medicine. 2014; 20:769–777.
18. Sato T, et al. Long-term Expansion of Epithelial Organoids From Human Colon, Adenoma, Adenocarcinoma, and Barrett's Epithelium. Gastroenterology. 2011; 141:1762–1772. [PubMed: 21889923]
19. van de Wetering M, et al. Prospective derivation of a living organoid biobank of colorectal cancer patients. Cell. 2015; 161:933–945. [PubMed: 25957691]
20. Boj SF, et al. Organoid Models of Human and Mouse Ductal Pancreatic Cancer. Cell. 2015; 160:324–338. [PubMed: 25557080]
21. Gao D, et al. Organoid Cultures Derived from Patients with Advanced Prostate Cancer. Cell. 2014; 159:176–187. [PubMed: 25201530]
22. Huch M, et al. Unlimited in vitro expansion of adult bi-potent pancreas progenitors through the Lgr5/R-spondin axis. The EMBO Journal. 2013; 32:2708–2721. [PubMed: 24045232]
23. Huch M, et al. In vitro expansion of single Lgr5+ liver stem cells induced by Wnt-driven regeneration. Nature. 2013; 494:247–250. [PubMed: 23354049]
24. Huch M, et al. Long-Term Culture of Genome-Stable Bipotent Stem Cells from Adult Human Liver. Cell. 2015; 160:299–312. [PubMed: 25533785]
25. Broutier L, et al. Culture and establishment of self-renewing human and mouse adult liver and pancreas 3D organoids and their genetic manipulation. Nat Protoc. 2016; 11:1724–1743. [PubMed: 27560176]

26. Brunt EM, P V, Sempoux C, Theise ND. Biphenotypic (hepatobiliary) primary liver carcinomas: the work in progress. Hepatic Oncology. 2015; 2:18.
27. Zhang F, et al. Combined hepatocellular cholangiocarcinoma originating from hepatic progenitor cells: immunohistochemical and double-fluorescence immunostaining evidence. Histopathology. 2008; 52:224–232. [PubMed: 18184271]
28. Zhao Y-J, Ju Q, Li G-C. Tumor markers for hepatocellular carcinoma. Molecular and Clinical Oncology. 2013; 1:593–598. [PubMed: 24649215]
29. Ohguchi S, et al. Expression of α-fetoprotein and albumin genes in human hepatocellular carcinomas: Limitations in the application of the genes for targeting human hepatocellular carcinoma in gene therapy. Hepatology. 1998; 27:599–607. [PubMed: 9462663]
30. Yakaboski E, Jares A, Ma Y. Stem cell gene SALL4 in aggressive hepatocellular carcinoma: a cancer stem cell-specific target? Hepatology. 2014; 60:419–421. [PubMed: 24327209]
31. Yong KJ, et al. Oncofetal gene SALL4 in aggressive hepatocellular carcinoma. N Engl J Med. 2013; 368:2266–2276. [PubMed: 23758232]
32. Moeini A, et al. Mixed hepatocellular cholangiocarcinoma tumors: Cholangiolocellular carcinoma is a distinct molecular entity. J Hepatol. 2017; 66:952–961. [PubMed: 28126467]
33. Shibata T, Aburatani H. Exploration of liver cancer genomes. Nature Reviews Gastroenterology & Hepatology. 2014; 11:340–349. [PubMed: 24473361]
34. Woo HG, et al. Identification of a cholangiocarcinoma-like gene expression trait in hepatocellular carcinoma. Cancer research. 2010; 70:3034–3041. [PubMed: 20395200]
35. Kalinich M, et al. An RNA-based signature enables high specificity detection of circulating tumor cells in hepatocellular carcinoma. Proc Natl Acad Sci U S A. 2017; 114:1123–1128. [PubMed: 28096363]
36. Kamlua S, et al. A novel TFF2 splice variant (ΔEX2TFF2) correlates with longer overall survival time in cholangiocarcinoma. Oncology Reports. 2012; 27:1207–1212. [PubMed: 22159958]
37. Banales JM, et al. Expert consensus document: Cholangiocarcinoma: current knowledge and future perspectives consensus statement from the European Network for the Study of Cholangiocarcinoma (ENS-CCA). Nat Rev Gastroenterol Hepatol. 2016; 13:261–280. [PubMed: 27095655]
38. Kraiklang R, et al. A novel predictive equation for potential diagnosis of cholangiocarcinoma. PLoS One. 2014; 9:e89337. [PubMed: 24586698]
39. Andersen JB, et al. Genomic and genetic characterization of cholangiocarcinoma identifies therapeutic targets for tyrosine kinase inhibitors. Gastroenterology. 2012; 142:1021–1031 e1015. [PubMed: 22178589]
40. Hsieh SY, et al. Stathmin1 overexpression associated with polyploidy, tumor-cell invasion, early recurrence, and poor prognosis in human hepatoma. Mol Carcinog. 2010; 49:476–487. [PubMed: 20232364]
41. Blokzijl F, et al. Tissue-specific mutation accumulation in human adult stem cells during life. Nature. 2016; 538:260–264. [PubMed: 27698416]
42. Zou S, et al. Mutational landscape of intrahepatic cholangiocarcinoma. Nat Commun. 2014; 5:5696. [PubMed: 25526346]
43. Totoki Y, et al. High-resolution characterization of a hepatocellular carcinoma genome. Nat Genet. 2011; 43:464–469. [PubMed: 21499249]
44. Li MM, et al. Standards and Guidelines for the Interpretation and Reporting of Sequence Variants in Cancer: A Joint Consensus Recommendation of the Association for Molecular Pathology, American Society of Clinical Oncology, and College of American Pathologists. J Mol Diagn. 2017; 19:4–23. [PubMed: 27993330]
45. Schulze K, et al. Exome sequencing of hepatocellular carcinomas identifies new mutational signatures and potential therapeutic targets. Nat Genet. 2015; 47:505–511. [PubMed: 25822088]
46. Borlak J, Meier T, Halter R, Spanel R, Spanel-Borowski K. Epidermal growth factor-induced hepatocellular carcinoma: gene expression profiles in precursor lesions, early stage and solitary tumours. Oncogene. 2005; 24:1809–1819. [PubMed: 15674348]

47. Jiao Y, et al. Exome sequencing identifies frequent inactivating mutations in BAP1, ARID1A and PBRM1 in intrahepatic cholangiocarcinomas. Nat Genet. 2013; 45:1470–1473. [PubMed: 24185509]
48. Li M, et al. Inactivating mutations of the chromatin remodeling gene ARID2 in hepatocellular carcinoma. Nat Genet. 2011; 43:828–829. [PubMed: 21822264]
49. Lee YT, Geer DA. Primary liver cancer: pattern of metastasis. J Surg Oncol. 1987; 36:26–31. [PubMed: 3041113]
50. Francies HE, Barthorpe A, McLaren-Douglas A, Barendt WJ, Garnett MJ. Drug Sensitivity Assays of Human Cancer Organoid Cultures. Methods Mol Biol. 2016
51. Morris EJ, et al. Discovery of a novel ERK inhibitor with activity in models of acquired resistance to BRAF and MEK inhibitors. Cancer Discov. 2013; 3:742–750. [PubMed: 23614898]
52. Iorio F, et al. A Landscape of Pharmacogenomic Interactions in Cancer. Cell. 2016; 166:740–754. [PubMed: 27397505]
53. Drexler HG, et al. p53 alterations in human leukemia-lymphoma cell lines: in vitroartifact or prerequisite for cell immortalization? Leukemia. 2000; 14:198–206. [PubMed: 10637496]
54. Frisch SM, Schaller M, Cieply B. Mechanisms that link the oncogenic epithelial–mesenchymal transition to suppression of anoikis. Journal of Cell Science. 2013; 126:21–29. [PubMed: 23516327]
55. Gu Q, et al. Genomic characterization of a large panel of patient-derived hepatocellular carcinoma xenograft tumor models for preclinical development. Oncotarget. 2015; 6:20160–20176. [PubMed: 26062443]
56. Hidalgo M, et al. Patient-derived xenograft models: an emerging platform for translational cancer research. Cancer Discov. 2014; 4:998–1013. [PubMed: 25185190]
57. Trapnell C, Pachter L, Salzberg SL. TopHat: discovering splice junctions with RNA-Seq. Bioinformatics. 2009; 25:1105–1111. [PubMed: 19289445]
58. Liao Y, Smyth GK, Shi W. featureCounts: an efficient general purpose program for assigning sequence reads to genomic features. Bioinformatics. 2014; 30:923–930. [PubMed: 24227677]
59. Love MI, Huber W, Anders S. Moderated estimation of fold change and dispersion for RNA-seq data with DESeq2. Genome Biol. 2014; 15:550. [PubMed: 25516281]
60. Subramanian A, et al. Gene set enrichment analysis: a knowledge-based approach for interpreting genome-wide expression profiles. Proc Natl Acad Sci U S A. 2005; 102:15545–15550. [PubMed: 16199517]
61. The UniProt, C. UniProt: the universal protein knowledgebase. Nucleic Acids Res. 2017; 45:D158–D169. [PubMed: 27899622]
62. Fang H, Gough J. The 'dnet' approach promotes emerging research on cancer patient survival. Genome Med. 2014; 6:64. [PubMed: 25246945]
63. Langmead B, Salzberg SL. Fast gapped-read alignment with Bowtie 2. Nat Methods. 2012; 9:357–359. [PubMed: 22388286]
64. McKenna A, et al. The Genome Analysis Toolkit: a MapReduce framework for analyzing next-generation DNA sequencing data. Genome Res. 2010; 20:1297–1303. [PubMed: 20644199]
65. Koboldt DC, et al. VarScan: variant detection in massively parallel sequencing of individual and pooled samples. Bioinformatics. 2009; 25:2283–2285. [PubMed: 19542151]
66. Cingolani P, et al. A program for annotating and predicting the effects of single nucleotide polymorphisms, SnpEff: SNPs in the genome of Drosophila melanogaster strain w1118; iso-2; iso-3. Fly (Austin). 2012; 6:80–92. [PubMed: 22728672]
67. Sherry ST, et al. dbSNP: the NCBI database of genetic variation. Nucleic Acids Res. 2001; 29:308–311. [PubMed: 11125122]
68. Lek M, et al. Analysis of protein-coding genetic variation in 60,706 humans. Nature. 2016; 536:285–291. [PubMed: 27535533]
69. Forbes SA, et al. COSMIC: exploring the world's knowledge of somatic mutations in human cancer. Nucleic Acids Res. 2015; 43:D805–811. [PubMed: 25355519]
70. Sim NL, et al. SIFT web server: predicting effects of amino acid substitutions on proteins. Nucleic Acids Res. 2012; 40:W452–457. [PubMed: 22689647]

71. Galili T. dendextend: An R package for visualizing, adjusting and comparing trees of hierarchical clustering. Bioinformatics. 2015; 31:3718–20. [PubMed: 26209431]

72. Colaprico A, et al. TCGAbiolinks: an R/Bioconductor package for integrative analysis of TCGA data. Nucleic Acids Res. 2016; 44:e71. [PubMed: 26704973]

73. Vis DJ, et al. Multilevel models improve precision and speed of IC50 estimates. Pharmacogenomics. 2016; 17:691–700. [PubMed: 27180993]

Europe PMC Funders Author Manuscripts

Europe PMC Funders Author Manuscripts

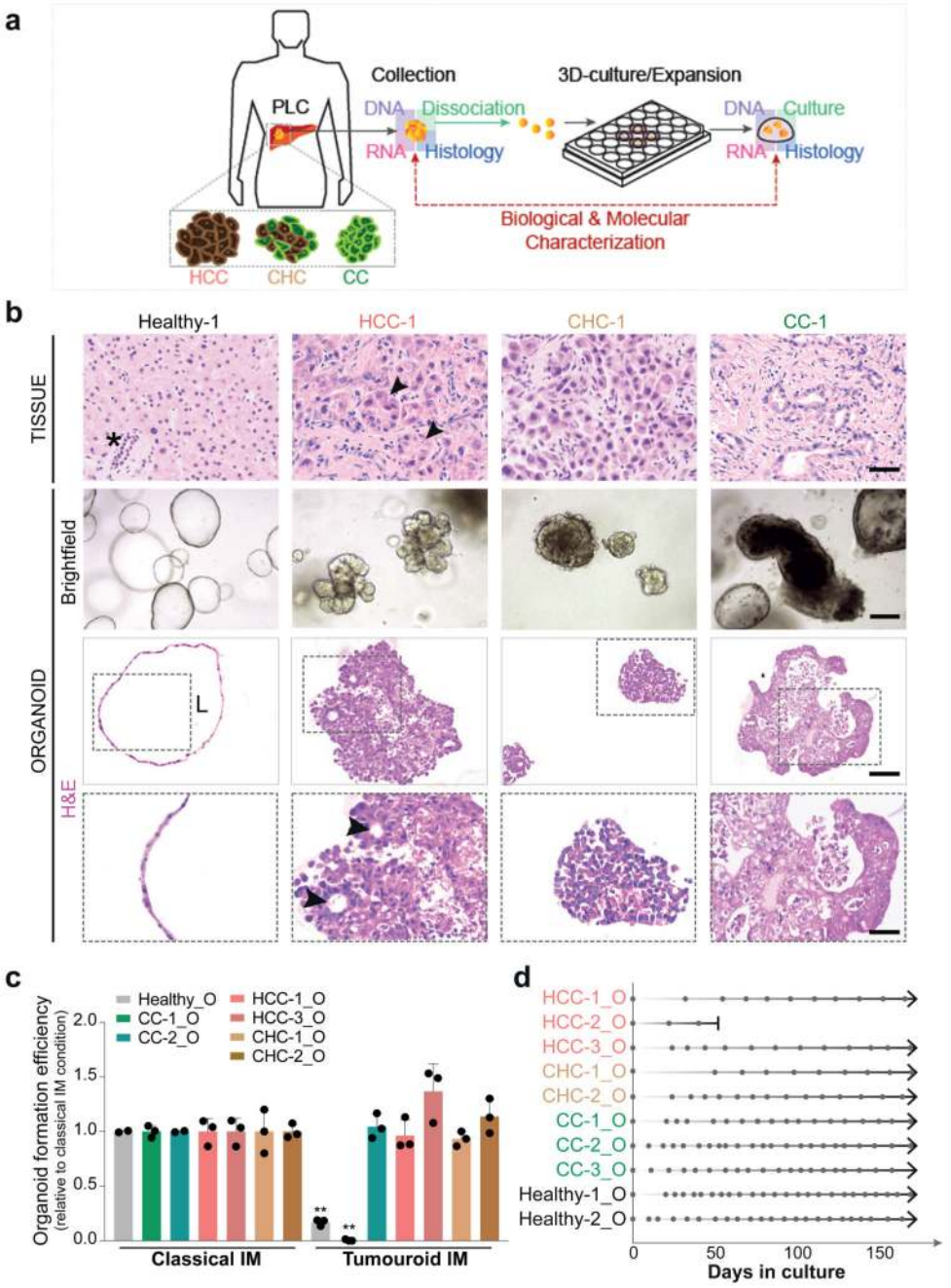

Figure 1. Patient-derived primary liver cancer organoid cultures expand long-term *in vitro* while preserving the histological architecture of the tumour subtype they derived from.

(a) Experimental design. Healthy (donor-derived) liver tissues, moderate/well differentiated hepatocellular carcinoma (HCC), combined hepatocellular-cholangiocarcinoma (CHC) and cholangiocarcinoma samples **(CC)** were obtained from patients undergoing surgery (patient's information detailed in Supplementary Table 1) and were processed as described in Methods and Supplementary Fig. 1. **(b)** Representative H&E staining of healthy liver tissue and primary tumours (top row), and corresponding brightfield microscopy images

Europe PMC Funders Author Manuscripts

(middle row) and H&E histological analysis of the organoid lines derived from these (bottom row). Note that, while healthy liver-derived organoids (left) grew as single layered epithelium of ductal-like cells surrounding a central lumen (*, duct; L, lumen), tumour-derived organoids (tumouroids; right) formed compacted structures that resembled the corresponding tumour-of-origin. HCC-1 tumouroids, like their parental tissue, exhibit pseudoglandular rosettes (arrowheads), a hallmark of HCC. CC-1 tumouroids present a glandular lumen, similar to the patient's tumour (top row). Scale bars, middle row 100μm; top and bottom rows, 50μm. Brightfield and H&E pictures from other lines are provided in Supplementary Fig. 2. **(c)** Organoid formation efficiency in classical human healthy liver isolation medium[24-25] and tumouroid specific isolation medium (classical human healthy liver isolation medium without Rspo-1, Noggin and Wnt3a and 3nM Dexamethasone - see methods and Supplementary Fig. 1 for details). Graph represents the mean±SD of the organoid formation efficiency in tumouroid IM relative to the one in classical IM. Individual data points are shown (circle). Significant differences between the classical and tumouroid IM groups were observed. **, p-value<0.001 (t-test, two-tailed). **(d)** Expansion potential of tumouroid cultures established and their correlation to the expansion of healthy-tissue derived organoids. Arrow, continuous expansion. Dot, passage.

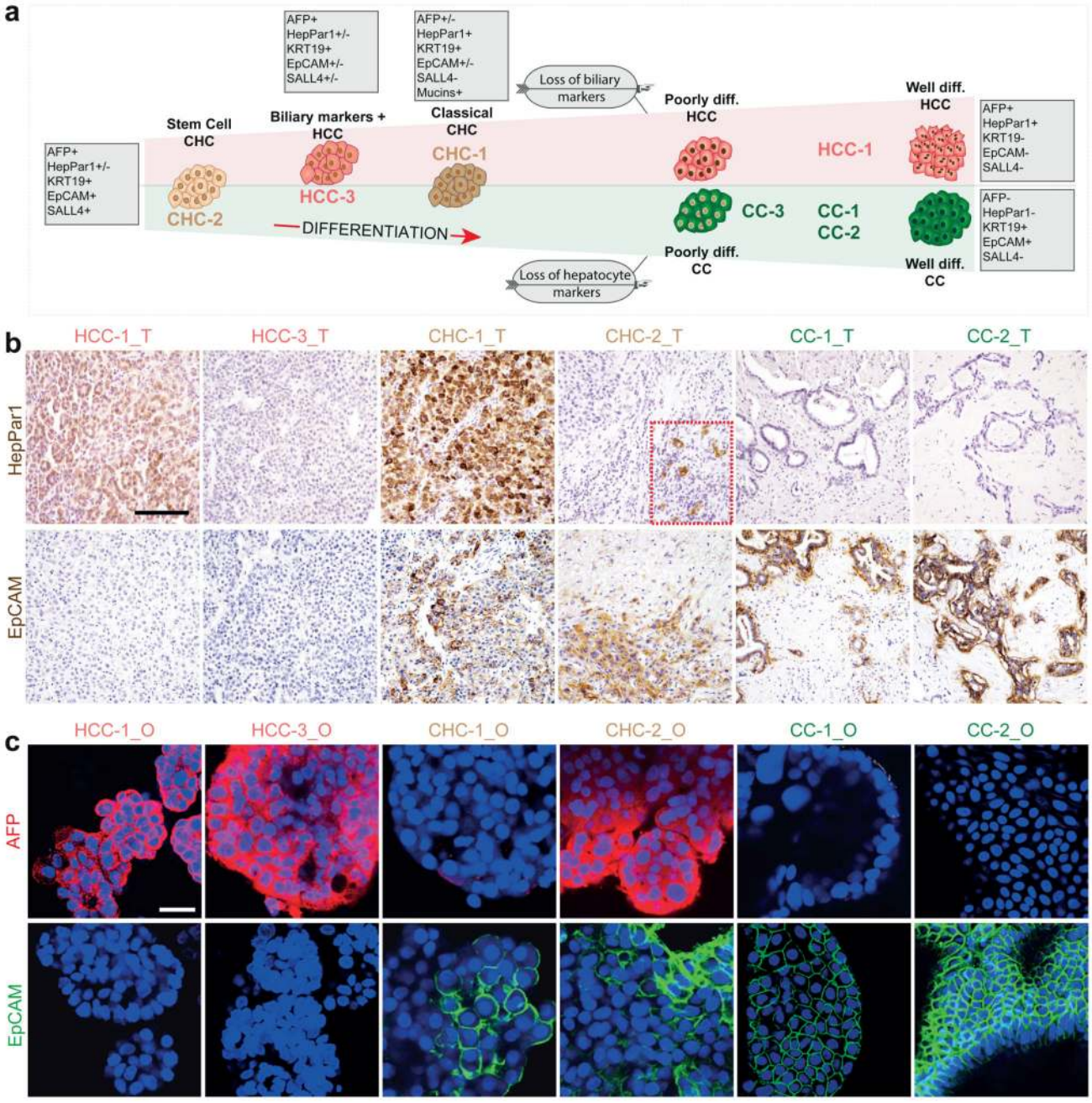

Figure 2. Immunohistochemistry analyses reveal that the PLC tumouroids retain expression patterns of the distinct subtype of the original tissue they derived from, even after long-term expansion in culture.

(a) Schematic representation of the multiple subtypes of primary liver cancers (PLC). **(b)** IHC assays on the PLC tissues including hepatocyte/HCC marker (HepPar1) and ductal/CC marker (EpCAM). Scale bar, 125 μm. Dashed red square indicates focal staining. **(c)** Immunofluorescent analysis for the HCC marker AFP (red) and the ductal/CC marker EpCAM (green), on tumouroids expanded in culture for at least 3 months. Nuclei were counterstained with Hoechst33342 (blue). Scale bar, 30μm.

Europe PMC Funders Author Manuscripts

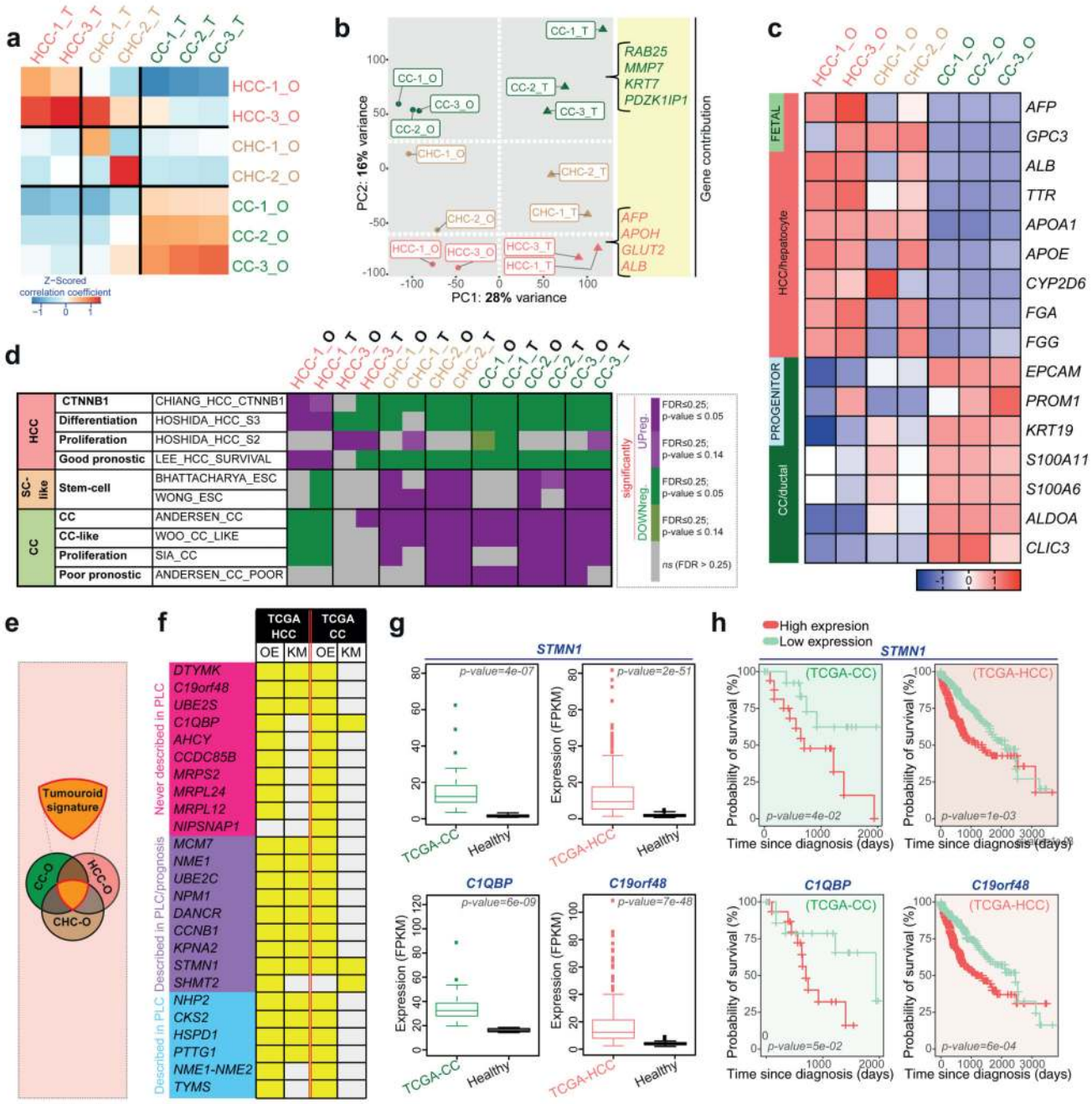

Figure 3. Tumouroids recapitulate the expression profiles of the specific tissue of origin.

(a) Correlation heat map between PLC-tissue (_T) and paired PLC-derived organoid line (_O) expression profiles' after at least >2 months expansion in culture. **(b)** Principal component analysis (PCA) showing samples plotted in 2 dimensions using their projections onto the first two principal components (PC1 and PC2). Each data point represents one sample (circle, tumouroid; triangle, tissue). PC1 is strongly correlated with the type of sample (tumouroids vs tissue) whereas PC2 defines the 3 different PLC subtypes (HCC, red; CHC, brown; and CC, green). Representative examples from the top-100 genes with highest

Europe PMC Funders Author Manuscripts

Europe PMC Funders Author Manuscripts

loadings across PC2 are shown. **(c)** Heat map analysis of the log2 RPKM values (raw z-scored) of selected genes found highly expressed (red) in HCC and/or CHC and/or CC tumouroids. Top left column indicates whether the indicated genes are markers of HCC/Hepatocyte/Fetal liver/CC/Ductal or liver progenitor markers. **(d)** Heat-map indicating representative gene-sets significantly (False discovery rate (FDR)<25%) UPregulated (purple) and DOWNregulated (green) in the tumouroid lines and paired tissues after performing gene set enrichment analysis (GSEA) comparing their gene signatures to 159 curated gene-sets associated with liver cancer and stem cell (representative plots are shown in Supplementary Fig. 5). Full list of gene-sets and significantly enriched gene-sets can be found in Supplementary Dataset 2 and 3. **(e)** Schematic of the tumouroid signature. Venn diagram overlapping the upregulated genes in each tumouroid line compared to healthy organoids. **(f)** Table summarizing the results of the gene expression (OE, overexpression) and outcome prediction (KM, Kaplan-Meier) analyses for the top 25-genes of the tumouroid signature using publically available TCGA cohorts. The table details the p-values obtained (OE, two-sided t-test ; KM, log-rank test). Statistical significance (p-value ≤0.05) is denoted by yellow color. Values for the top 30-genes can be found in Supplementary Dataset 1. TCGA-HCC, 374 tumour/50 normal samples; TCGA-CC, 31 tumour/8 normal samples. **(g)** Expression of *STMN1*, *C1QBP* and *C19orf48* in tumour and normal tissues in the TCGA-HCC and/or CC cohorts. Center line, median; box plot, interquartile range (IQR); whiskers, range (minimum to maximum). **(h)** Kaplan-Meier analyses of the TCGA-HCC and/or TCGA-CC cohorts based on the expression level of the indicated genes in the cohorts samples.

Europe PMC Funders Author Manuscripts

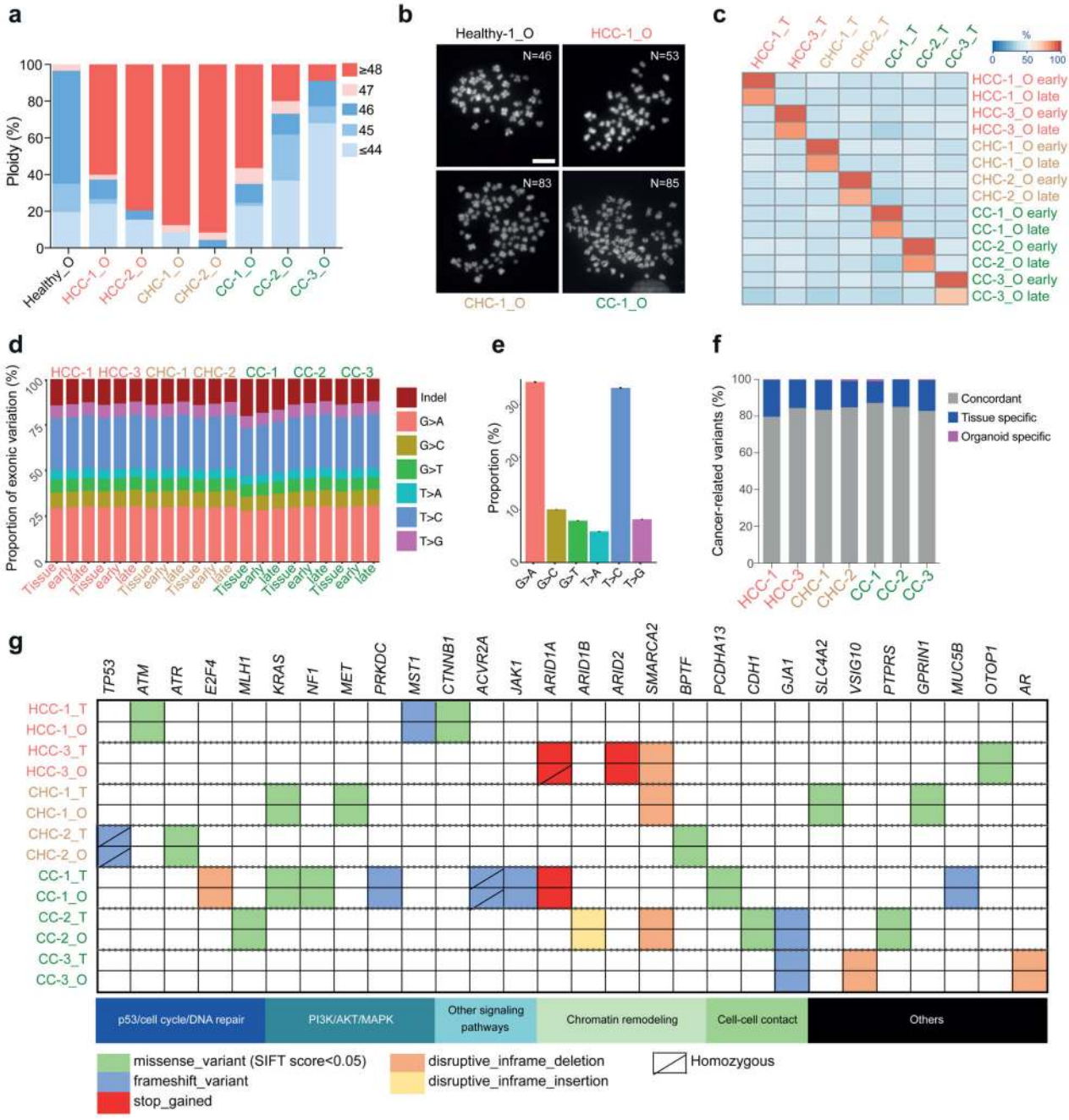

Figure 4. Tumouroids preserve the genetic alterations from the original tumour

(a) Ploidy analysis of tumouroid cultures expanded for at least 2 months in culture. Results are expressed as % of ploidy per number of metaphases counted (at least 21 total). Healthy-derived organoids were used as control. A minimum of two independent experiments were performed. **(b)** Representative images of organoid metaphases used for the ploidy analysis. Scale bar, 10μm. **(c-e)** Whole exome sequencing analysis of patient's tumour tissues and corresponding tumouroid cultures expanded for < 2 months (early passage) or >4 months (late passage) in culture. All variants identified in all samples (21 total; 7 patients with 3

samples each (Tissue/early organoid/late organoid) were used for the global analyses after filtering for quality control as detailed in methods). **(c)** Correlation heat-map between the variants identified in PLC-tissues (_T) and PLC-tumouroids (_O). **(d)** Proportions of exonic variants across the samples, the 6 types of SNVs and the Indels are represented. **(e)** Percentage of the 6 types of SNVs averaged across all samples. Graph represents mean±SD. **(f-g)** A cancer-related set of variants **(f)** and variants predicted to impair protein function (SIFT score <0.05 filter) **(g)** were identified as described in methods. **(f)** Bar plots indicate the concordance (%) between the cancer-related variants identified in the tumour-of-origin and the corresponding tumouroids expanded for short term in culture. **(g)** Damaging coding mutations found in genes already described mutated in liver cancer (Full list is found in Supplementary Dataset 4, spread sheet 15 details the references). The type of mutation is indicated in the legend. _T, tissue; _O, organoid.

Europe PMC Funders Author Manuscripts

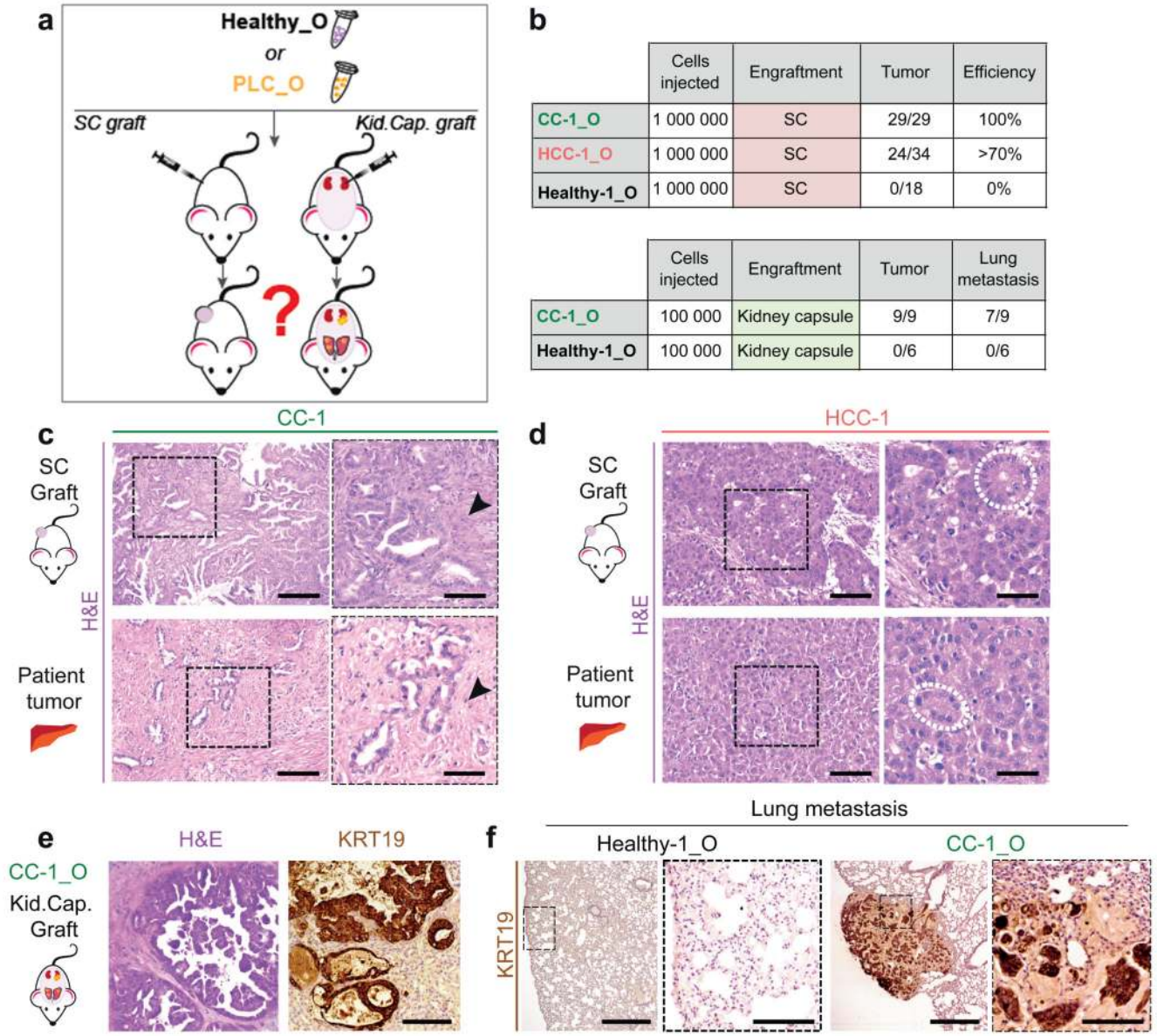

	Cells injected	Engraftment	Tumor	Efficiency
CC-1_O	1 000 000	SC	29/29	100%
HCC-1_O	1 000 000	SC	24/34	>70%
Healthy-1_O	1 000 000	SC	0/18	0%

	Cells injected	Engraftment	Tumor	Lung metastasis
CC-1_O	100 000	Kidney capsule	9/9	7/9
Healthy-1_O	100 000	Kidney capsule	0/6	0/6

Figure 5. ***In vivo*** **growth and metastatic potential of PLC tumouroids**

(a) Experimental design. PLC tumouroids or Healthy liver-derived organoids expanded for >3 months in culture were transplanted subcutaneously (SC) or under the kidney capsule (Kid.Cap.) of immunocompromised NSG mice and analysed for the presence of tumour growth and metastasis following grafting. **(b)** Tables summarizing the number of cells, site of engraftment and analysis of tumour and lung metastasis. No tumour lesions were found in any of the mice injected with Healthy-1 organoids. **(c-d)** Representative H&E staining of CC-1 **(c)** and HCC-1 **(d)** tumouroids transplanted subcutaneously (top) into NSG mice and corresponding patient's tumour sample (bottom). **(c)** Note that the grafted CC-1 tumouroid tissue (top) recapitulates the histo-architecture of the patient's original tumour (bottom) including the extensive desmoplastic reaction (arrowheads). Scale bars, left 125μm, right 62.5μm. **(d)** Note that the grafted HCC-1 tumouroid tissue recapitulates the histo-

Europe PMC Funders Author Manuscripts

architecture of the patient's original tumour (bottom) including the pseudoglandullar rosettes, hallmark of HCC-1 original sample (dashed circle). Scale bars, left 125μm, right 62.5μm. **(e)** Representative H&E (left) and KRT19 (right) immunohistochemistry analyses of CC-1 tumouroids transplanted under the kidney capsule of NSG mice. Scale bar, 125μm. **(f)** Lung metastases derived from CC-1 tumouroids transplanted under the kidney capsule (right panels) were identified using a human specific KRT19 antibody. No metastases were found in the lungs of mice injected with Healthy-1 organoids (left panels). Scale bars, 500μm, magnifications 125μm.

Europe PMC Funders Author Manuscripts

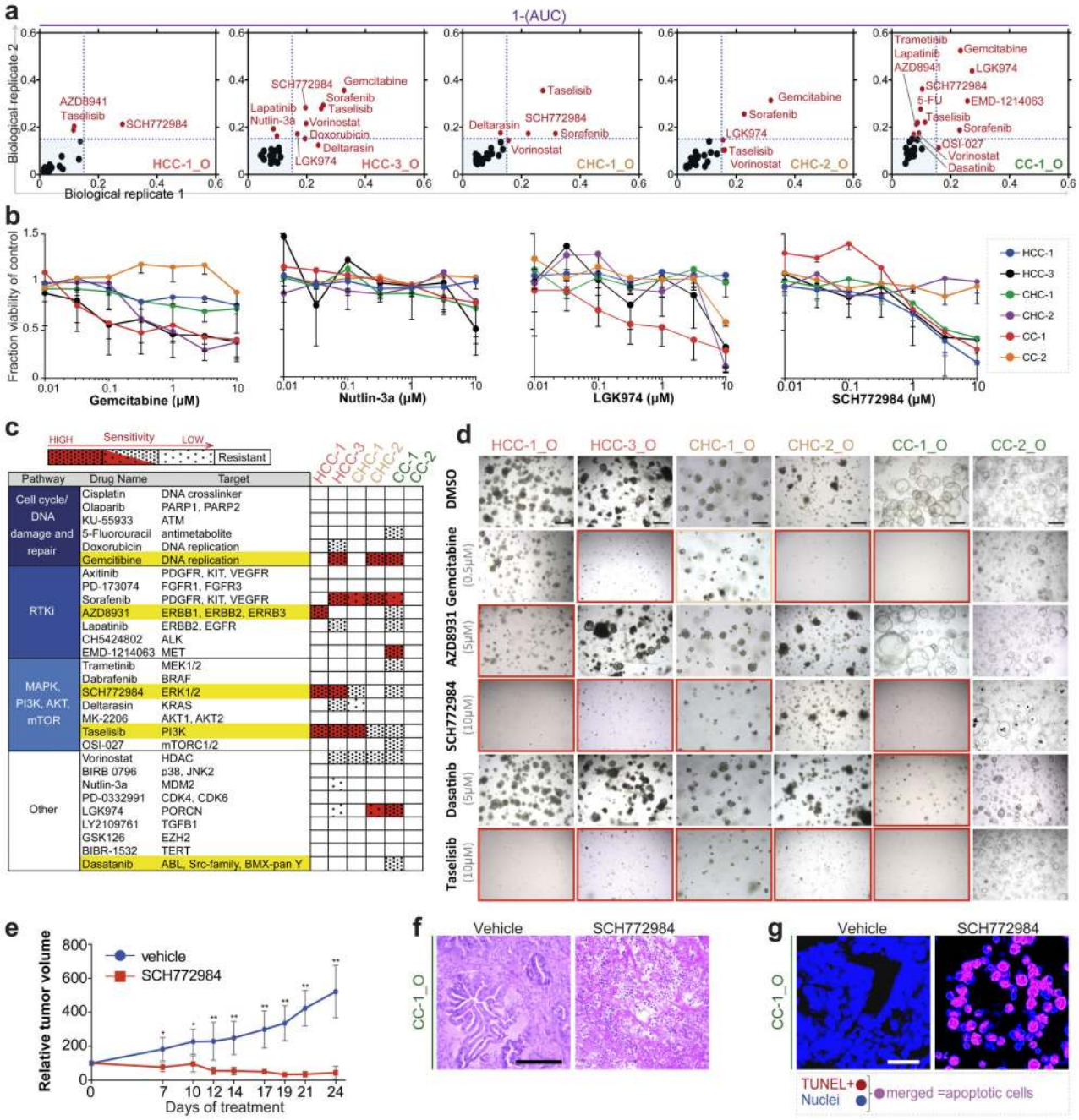

Figure 6. PLC tumouroid lines as a platform for drug screening and validation of actionable therapeutic targets.

(a) Scatterplot of 1-AUC (Area Under the Curve) values from two biological replicates (different passages) of the drug screening data, highlighting drugs (red) having a potential effect on viability (AUC >0.15 for at least 1 of the two replicates) in the indicated tumouroid lines. Each data point is the 1-AUC value for a given drug in a particular tumouroid line. **(b)** Dose-response curves after 6 days treatment with Gemcitabine, Nutlin-3a, LGK974 and SCH772984 generated from the luminescent signal intensities. Data displayed are average of

Europe PMC Funders Author Manuscripts

the technical and biological replicates. **(c)** Summary of the different compounds used in the drug screening, the associated pathway and nominal targets and the screen results represented as a summary of the 1-AUC and IC50 data generated for the different tumouroid lines. Red, IC50 within the screen concentration range (detailed in methods); Dense dotted pattern, 1-AUC>0.15 and dose response; scattered dotted pattern, 1-AUC>0.15 and sensitivity at highest concentration only (Supplementary Dataset 5). Compounds highlighted in yellow were selected for further validation. **(d)** Effects on viability of indicated compounds using an organoid formation assay (detailed in methods). Red square, no viable cells; orange square, intermediate sensitivity; no square, resistant. Scale bar, 500μm. **(e)** *In vivo* activity of the ERKi (SCH772984) in CC-1_O tumouroids grafted subcutaneously in NSG mice. Mice were treated with drug/vehicle twice daily for 20 days (n=5 in 2mg/kg of SCH772984 group, n=8 in vehicle group). *, p-value<0.01; **, p-value<0.002 (Mann Whitney test, two-tailed). Results are shown as percentage of the tumour volume relative to day 0 (mean ±SD). **(f-g)** Histological analysis of the antitumor efficacy of SCH772984 on CC-1_O tumours was assessed 24 days after starting the treatment. Representative **(f)** H&E and **(g)** TUNEL staining performed on tissue sections from CC-1_O tumours treated with either vehicle (left) or SCH772984 (right). Representative images from 2 independent experiments are shown. Scale bar, 125μm (H&E) and 25μm (TUNEL).

Europe PMC Funders Author Manuscripts